

Organic carbon burial dynamics at the Chukchi Shelf margin: Implications for the Arctic Ocean carbon sink

Liming Ye^{a,*}, Xiaoguo Yu^a, Yanguang Liu^b, Anatolii S. Astakhov^c, Alexander Bosin^c,
Yeping Bian^a, Linsen Dong^b, Weijia Fan^a, Haili Yang^d

^a Key Laboratory of Submarine Geosciences & Second Institute of Oceanography, Ministry of Natural Resources, Hangzhou 310012, China

^b Key Laboratory of Marine Geology and Metallogeny & First Institute of Oceanography, Ministry of Natural Resources, Qingdao 266061, China

^c V.I. Il'ichev Pacific Oceanological Institute, Far Eastern Branch of the Russian Academy of Sciences, 43 Baltiyskaya St., Vladivostok 690041, Russia

^d Analysis and Test Center, Third Institute of Oceanography, MNR, Xiamen, China

ARTICLE INFO

Editor: M Elliot

Keywords:

Suspended particulate material
Organic carbon burial
Carbon sink
Chukchi Shelf
Arctic Ocean

ABSTRACT

Organic carbon (OC) burial plays a crucial role in regulating the Arctic Ocean's capacity to uptake atmospheric CO₂. In this study, we demonstrate the transport, deposition, and degradation patterns of different sources of OC to reveal burial dynamics at the Chukchi Shelf margin, a region with the highest primary production in the Arctic Ocean currently affected by dramatic sea ice retreat. Observations of suspended particulate material show a pronounced separation of terrestrial and marine OC in the water column, which subsequently influences OC lateral transport and differential deposition. Easily suspendable terrestrial OC is concentrated in the upper 10 m of water or sea ice and transported to the Canada Basin, where it undergoes severe degradation of fresh carbon in the water column and uppermost sediments. In contrast, faster-settling marine OC is more likely to be buried in the canyons and at the Chukchi Shelf margin, with ice algae contributing about 14 % and 55 % of OC burial in areas south and north of 73°N, respectively, leading to higher initial burial efficiency. Increasing Arctic marine primary production could thus enhance the region's role as a carbon sink over millennial timescales, although the burial efficiency of terrestrial OC will eventually exceed that of marine OC with prolonged burial time. Our findings highlight the importance of lateral transport, differential deposition, and selective degradation in Arctic carbon burial, providing a basis for objectively assessing the future capacity of the Arctic carbon sink and its feedback to climate change.

1. Introduction

Organic carbon (OC) burial in marine sediments represents a dominant mechanism for long-term carbon sequestration and can efficiently regulate the atmospheric CO₂ budget (Cartapanis et al., 2016; Faust et al., 2021; Li et al., 2023). With global warming, the broad shelves and even the entire Arctic Ocean may no longer have perennial sea ice within several decades, potentially becoming the world's most significant new carbon sink due to increased primary production and subsequent OC burial (Bates, 2006; Jahn et al., 2024; Harada, 2016; Peng et al., 2020; O'Daly et al., 2020). However, the long-term carbon sequestration is not always driven by primary production, as most marine OC is extensively degraded in the water column or sediments and is subsequently released back into the ocean-atmosphere carbon pool (Cartapanis et al., 2016; Stein and Macdonald, 2004; Yamamoto et al., 2008). Furthermore, the

burial of terrestrial OC, while significant, does not enhance the Arctic Ocean's capacity to absorb atmospheric CO₂ (Martens et al., 2019). Instead, this process highlights the remobilization and degradation of permafrost carbon, which undermines the potential for the Arctic Ocean to act as an effective carbon sink when it enters the marine environment (Semiletov et al., 2016). Continuous feedback from the degradation of marine and terrestrial OC during and after burial increases the uncertainty of the Arctic Ocean as an effective carbon sink. The extent and duration of organic carbon burial driving Arctic Ocean carbon sinks, as well as future trends in organic carbon burial, remain poorly understood.

The most robust Arctic marine response to global warming has occurred in and around the Chukchi Sea (Fig. 1: Peng et al., 2020). This response signals what might happen throughout the Arctic shelves within several decades. The Chukchi Sea is characterized by high

* Corresponding author.

E-mail address: lmye@sio.org.cn (L. Ye).

<https://doi.org/10.1016/j.palaeo.2024.112534>

Received 25 May 2024; Received in revised form 29 August 2024; Accepted 1 October 2024

Available online 9 October 2024

0031-0182/© 2024 Elsevier B.V. All rights reserved, including those for text and data mining, AI training, and similar technologies.

primary production, with export rates averaging 82 %, but most of the OC produced and introduced is not buried in situ (Astakhov et al., 2013; Bates, 2006; Hill et al., 2018; O'Daly et al., 2020). The lateral transport of particulate OC from the Chukchi Shelf to the basin appears to be the primary control on the subsequent deposition and burial of marine and terrestrial OC (Liu et al., 2023; Xiang and Lam, 2020). Theoretically, significant lateral transport is detrimental to OC burial because degradation begins in the water column, and the amount of OC reaching the seafloor decreases exponentially with water depth (Burdige, 2007; Darby et al., 2009; Heip et al., 1995). Although up to 95 % of the buried OC still tends to degrade, it can persist for thousands of years or more, showing better sustainability than in the water column (Coffin et al., 2017; Faust et al., 2021). If marine OC and permafrost carbon can be preferentially deposited before entering the deep basin, this would positively feedback to the Arctic carbon sink. Higher-resolution observations are needed to characterize the lateral transport and deposition of particulate OC in the broad Bering-Chukchi shelf, as approximately 60 % of the sediments on the Chukchi Shelf are imported by the Bering Strait inflow (Astakhov et al., 2019; Liu et al., 2023; Viscosi-Shirley et al., 2003).

Receding perennial sea ice at the Chukchi Shelf margin has caused measurable changes in phytoplankton communities, increases in primary production, and potentially affects OC deposition and burial (Boetius et al., 2013; Hill et al., 2018; Watanabe et al., 2014). As documented at the northern Chukchi Shelf margin, ice algae mainly

bloom under sea ice and then sink to the seafloor with sea ice retreat from May 15th to June 15th, preceding the large-scale input of terrestrial OC and other phytoplankton (Arrigo et al., 2014; Stabeno et al., 2020). Over the northern Chukchi Sea, it is estimated that ice algae contribute more than 50 % of primary production, and the export rate of ice algae may exceed 85 % (Boetius et al., 2013; Clement Kinney et al., 2020). The thinning sea ice and increasing melt-pond cover may continue to enhance under-ice production and ice algae export in the future (Arrigo et al., 2012). Whether in the deposition process or the ice algae production, these new findings will change the original understanding of OC burial and need to be verified from the sedimentary records. The problem is that accurately identifying ice algae and other sources of OC in sediments has always been challenging in studying OC burial. If the marine $\delta^{13}\text{C}$ end member (EM) in the mixing model can be defined more precisely, the big data of $\delta^{13}\text{C}_{\text{Org}}$ accumulated over the past decades in the study area will fully play its advantages. The processes related to the OC source, transport, deposition, and degradation could be widely explored under the current conditions.

In this study, we first aim to elucidate the OC transport and deposition through modern observations. Furthermore, we re-evaluate marine $\delta^{13}\text{C}_{\text{Org}}$ data to enhance the accuracy of the EM mixing model, reconstruct the degradation and burial patterns of marine and terrestrial OC separately, and then demonstrate the dynamics of OC burial since the Holocene. The analyzed proxies, including SPM concentration, OC content, and isotopic composition ($\delta^{13}\text{C}_{\text{Org}}$ and $\Delta^{14}\text{C}_{\text{Org}}$), are based on an

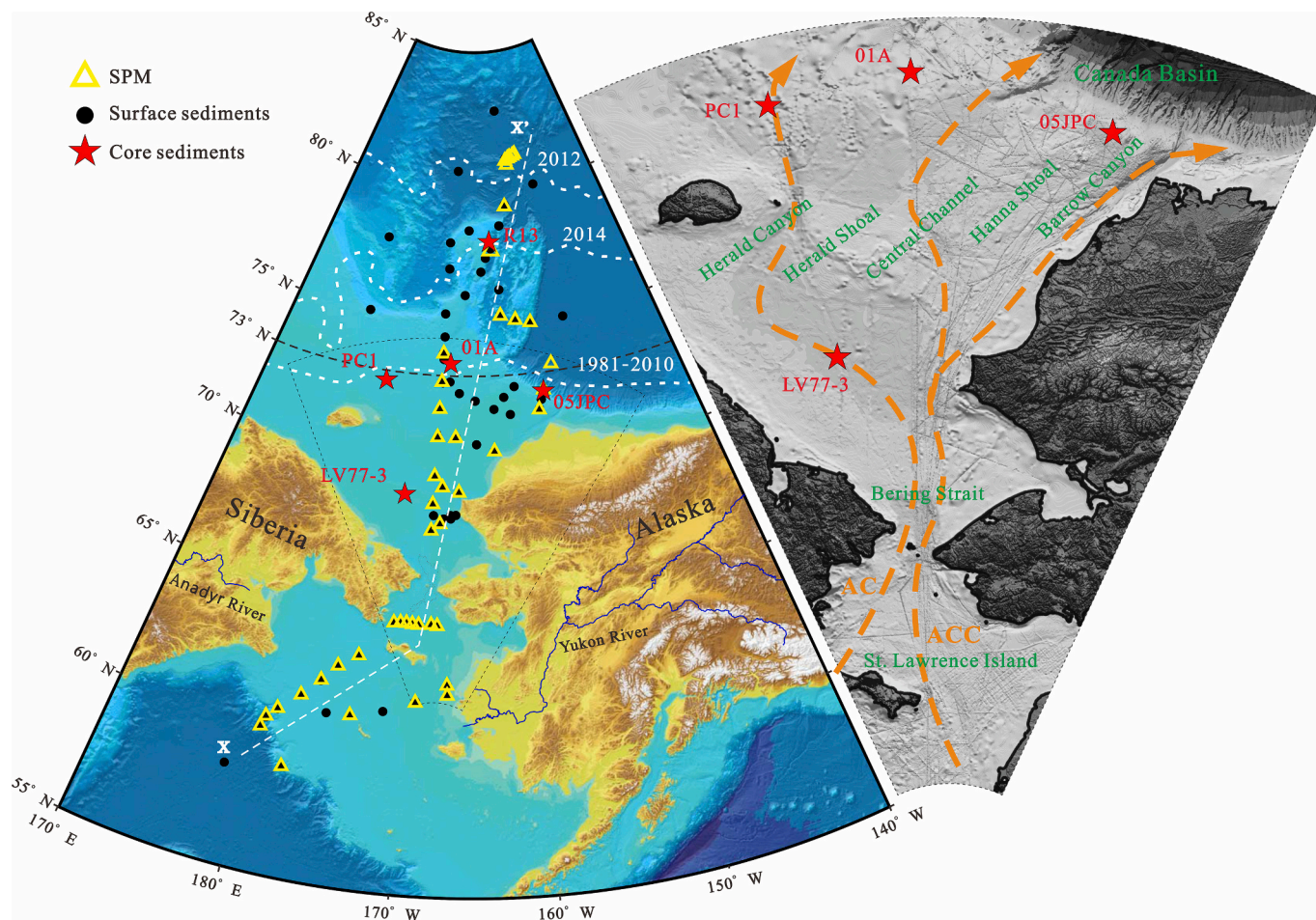


Fig. 1. Geographic setting and sampling locations. Yellow triangles represent sampling sites for SPM, black dots for surface sediments, and stars for core sediments. White dashed lines indicate the sea ice extent minimum (15 % ice concentration) for the 30-year (1981–2010), the 2012, and the 2014 (Arguez et al., 2012; Melsheimer and Spreen, 2019). Black dashed line highlights 73°N. Brown dashed lines with AC and ACC represent the Anadyr Current and Alaska Coastal Current, respectively (Corlett and Pickart, 2017). Dashed white line X-X' indicates water depth profile shown in Fig. 2. (For interpretation of the references to colour in this figure legend, the reader is referred to the web version of this article.)

extensive new data set and previous studies (Jakobsson et al., 2017; Martens et al., 2019; McKay et al., 2008; Swärd et al., 2018; Yu et al., 2023). The SPM, surface sediments, and core sediment samples were collected from the northern Bering Sea, Chukchi Sea, and adjacent Canada Basin, regions where the response to ongoing global warming provides insights into the future state of the Arctic Ocean.

2. Regional background

2.1. Geographic setting

Between the Bering Shelf and the Chukchi Shelf, the Bering Strait opens and closes periodically with sea level changes during glacial-interglacial cycles. The last opening occurred around 11,000 years ago (Jakobsson et al., 2017). Since then, the Bering Strait inflow has become an essential part of the global thermohaline circulation and impacts regional primary production (Hu et al., 2010; Liu et al., 2023; Stein and Macdonald, 2004). Under the combined influence of tectonics, ocean currents, sea level, and glaciers, the Chukchi Shelf developed a topography of alternating canyons and shoals. From west to east, these include the Herald Canyon, the Herald Shoal, the Central Channel, the Hannah Shoal, and the Barrow Canyon (Fig. 1). The Alaska Coastal Current and the Anadyr Current enter the Chukchi Sea through the Bering Strait, differing in salinity, nutrient content, oxygen levels, and depth, and then divide into three branches (Fig. 1; Pickart et al., 2010). One branch flows north along the Herald Canyon, mainly from the Anadyr Current, another flows along the Central Channel, and the most significant flow from the Alaska Coastal Current enters the Barrow Canyon (Fig. 1). These currents eventually turn east and enter the Beaufort Sea and the Canada Basin, forming the upper halocline above the Atlantic water layer.

2.2. Hydrodynamics and sea ice

A large amount of sediment on the Chukchi Shelf is imported by the Bering Strait inflow due to its strong hydrodynamics (Fig. 1; Astakhov et al., 2019; Liu et al., 2023; Viscosi-Shirley et al., 2003). The sediment-laden Bering Strait inflow occurs in winter but is more intense in summer (Woodgate, 2018). Its velocity typically ranges between 20 and 50 cm/s, with a maximum of 100 cm/s, gradually decreasing towards the north (Abe et al., 2019; Woodgate, 2018). At the junction of the Chukchi and Beaufort shelves, the bottom current velocity is about 5–20 cm/s, which can intermittently suspend coarse silt (45–63 μm) (Coachman and Aagaard, 1966; Darby et al., 2009). The Bering Strait inflow reached its peak in the mid-Holocene (between approximately 6 and 4 ka) (Ortiz et al., 2009; Polyak et al., 2016). High inflow volumes favor the westward diversion of more Pacific water at the expense of diminished Alaska Coastal Current contributions (Winsor and Chapman, 2004).

A visible response to the increasing volume of inflow is the retreat of sea ice (Abe et al., 2019; Melsheimer, 2019). Near the Chukchi Plateau, year-round sea ice may have begun forming around 100 ka (Lazar and Polyak, 2016). After entering the Holocene, the front of perennial sea ice fluctuated roughly along the Chukchi Sea margin (Polyak et al., 2016). Sea ice coverage in the northern Bering Sea reaches its maximum at the end of March each year and then gradually recedes northward, reaching its low point in early September (Walt et al., 2020). Recently, the area of ice-free water has continued to expand further north of the Chukchi Sea, with a strengthening inflow (Abe et al., 2019; Walt et al., 2020).

2.3. Organic sources and $\delta^{13}\text{C}_{\text{org}}$

Around the Chukchi Sea, diatoms and dinoflagellates are the main phytoplankton species, influenced by sea ice and nutrient availability (Astakhov et al., 2020; Obrezkova and Pospelova, 2019; Stein et al., 2017). The Chukchi Sea supports primary production of up to 166 $\text{gC}/\text{m}^2/\text{yr}$, significantly higher than the 7–28 $\text{gC}/\text{m}^2/\text{yr}$ recorded in the

central Arctic Ocean (Boetius et al., 2013; Moran et al., 1997; Watanabe et al., 2014). Since 2003, the retreat of sea ice has led to an Arctic-wide increase in primary production, estimated at 27.5 TgC/yr , predominantly in the Chukchi and Siberian Seas (Arrigo et al., 2008; Hill et al., 2018). The peak primary production period in the Hannah Shoal spans from July to October, while on the Northwind Ridge, it is slightly shorter, from August to October (Lalande et al., 2020; Ren et al., 2020; Watanabe et al., 2014). Recent observations and simulations indicate that the contribution of under-ice production is much more significant than initially thought (Arrigo et al., 2014; Boetius et al., 2013; Clement Kinney et al., 2020; Stabeno et al., 2020). The marine $\delta^{13}\text{C}_{\text{org}}$ at high latitudes typically ranges between -30.4‰ and -16.7‰ (Stein and Macdonald, 2004). The average value of phytoplankton $\delta^{13}\text{C}_{\text{org}}$ in the open waters of the East Siberian Sea is about -21‰ , which is defined as the marine $\delta^{13}\text{C}_{\text{org}}$ EM in the study area (Martens et al., 2019). Ice algae have a heavier $\delta^{13}\text{C}_{\text{org}}$ ranging from -15 to -8‰ (Stein and Macdonald, 2004). The $\delta^{13}\text{C}_{\text{org}}$ in bulk sediments is often $> -21\text{‰}$ and is thought to be influenced by ice algae, contributing about 5–10% (Goñi et al., 2005; Naidu et al., 2000). Considering the effects of ice algae, the marine $\delta^{13}\text{C}_{\text{org}}$ EM was redefined as -17.5‰ (Belicka and Harvey, 2009). Another source of $\delta^{13}\text{C}_{\text{org}}$ is bacteria, such as green sulfur bacteria, which range from -15 to -10‰ (Pearson et al., 2001). In the Chukchi Sea, the ratio of bacterioplankton to phytoplankton production varies with an average of 0.34, insufficient to shift the $\delta^{13}\text{C}_{\text{org}}$ by more than 1‰ (Cooper et al., 2015).

No large rivers discharge directly into the Chukchi Sea. The terrestrial OC entering the Chukchi Sea primarily comes from the Yukon and Anadyr rivers, runoff, and coastal erosion (Guo and Macdonald, 2006; Stein and Macdonald, 2004). OC from the Siberian rivers and the Mackenzie River is also partially imported via ocean currents and sea ice (Naidu et al., 2000; Semiletov et al., 2016). Based on fatty acid analysis, the terrestrial OC in the Chukchi Shelf, continental slope, and northern basin sediments account for 62%, 96%, and 44% of the total buried OC, respectively. However, $\delta^{13}\text{C}_{\text{org}}$ and lipid biomarkers result in much lower estimates, between 11% and 44% (Belicka and Harvey, 2009; Belicka et al., 2004a, 2004b). The $\delta^{13}\text{C}$ of land plants utilizing the C3 photosynthetic pathway ranges from -28‰ to -26‰ , but the degradation of labile components can enrich the ^{13}C signal (Drenzek et al., 2007; Søreide et al., 2006; Naidu et al., 2000; Soong et al., 2021). The terrestrial $\delta^{13}\text{C}_{\text{org}}$ in ice-complex deposits in Eastern Siberia is -32.1‰ , in topsoil permafrost is -26.3‰ , and the mixed $\delta^{13}\text{C}_{\text{org}}$ is -27.5‰ (Semiletov et al., 2016; Vonk et al., 2010). The terrestrial $\delta^{13}\text{C}_{\text{org}}$ in Alaska's northern river delta is about -27.8‰ (Belicka and Harvey, 2009). Multiple sources mixed to an average $\delta^{13}\text{C}_{\text{org}}$ of about -27.1‰ , defined as the terrestrial $\delta^{13}\text{C}_{\text{org}}$ EM in the study area (Martens et al., 2019).

3. Materials and methods

3.1. Suspended particulate material

SPM samples were collected during the 6th Chinese National Arctic Research Expedition (CHINARE) 2014 field season, from July 21st to August 24th, aboard the RV Xuelong (Yu et al., 2023). Four McLane large volume water transfer systems (model WTS 6–1–142LV) were deployed at 47 sites at water depths of 20 (one site at 30), 50, 100, and 150 m, totaling 141 samples. The SPM was collected simultaneously from all sampling layers at each site, with a sampling duration of 30 min. The sampler was placed almost vertically with the inlet on the side, which may have resulted in larger quantities and coarser composition of the collected SPM in areas with strong horizontal transport, such as the Bering Strait, while coarse particles could be underestimated in areas dominated by vertical deposition. Surface water SPM was collected using a bucket from the ship's starboard side (the drain is on the port side).

The study area extended from the northern Bering Sea across the

Chukchi Sea and Borderland into the Canada Basin (Fig. 1). Most samples were collected in open water, except for sites north of 77°N, where SPM was collected after breaking the sea ice. Long-term observations were conducted at six sites north of 80°N (LIC1–LIC6), where the RV Xuelong drifted with the sea ice from August 18th to 24th, collecting SPM once a day. After removing the sampler from the water, it was transferred to the onboard laboratory, where deionized water was used to wash away salt from the filter membrane (Whatman GF/F with a pore size of 0.7 μm). The filter membrane was then removed, wrapped in tin foil, and stored in a refrigerator at –20 °C.

Our samples were augmented by the data of Bates et al. (2005), Goñi et al. (2021), and Xiang and Lam (2020), which were based on compatible SPM sampling in the same region, including near-seabed samples in the Bering Strait area.

3.2. Sediments

Fifty-six surface-sediment samples were collected from the seabed (0–5 cm) during the 6th and 7th CHINARE expeditions in 2014 and 2016. The sampling sites closely correspond to the SPM collection sites (Fig. 1). Samples were stored at –20 °C in a refrigerator until analysis. For data re-analysis, we also utilized 503 surface-sediment samples from previous studies (Astakhov et al., 2019; Grebmeier and Cooper, 2019; Martens et al., 2021; Naidu et al., 2000).

A gravity sediment core, LV77–3, was recovered in 2016 by the “Arctic Silk Way” Russian-Chinese Expedition from the inner Chukchi Shelf (Fig. 1). Multiple sedimentary proxies have been reported for core LV77–3 by Astakhov et al. (2020). In this study, LV77–3 samples taken at 4-cm increments were used for measuring TOC and $\delta^{13}\text{C}_{\text{org}}$. Additionally, we used sedimentary proxy data from several prior studies, including gravity sediment core ARA2B-01 A (hereafter 01 A) and piston core SWERUS-L2–4-PC1 (hereafter PC1) from the outer Chukchi Shelf (Stein et al., 2017; Martens et al., 2019), and piston core HLY0501-05JPC (hereafter 05JPC) from the Chukchi Slope (Fig. 1; McKay et al., 2008).

3.3. Analytical methods

The membrane samples were freeze-dried and weighed. Based on seven blank filter membranes, the weight of SPM was calibrated and then divided by the volume of the filtered water to obtain the SPM concentration (mg/L). About 1/16 of the filter membrane was used to analyze the total organic carbon (TOC) and stable carbon isotope ($\delta^{13}\text{C}_{\text{org}}$) following the method by Hilton et al. (2010). Carbonate-free samples were converted to gas by combustion in an elemental analyzer (Thermo NE1112) connected to a Thermo Finnegan Delta plus AD mass spectrometer by a ConFlo III interface. Reference materials USGS-24, GBW4408, and IAEA-N1 were used to calibrate the pure CO_2 from the laboratory tank. As a result, the particulate organic carbon (POC) concentration was calculated from the SPM concentration and TOC. The reproducibility of TOC (at the 1 σ level) was 0.04 %, and the analytical precision of $\delta^{13}\text{C}_{\text{org}}$ (at the 1 σ level) was about 0.2 %.

All surface-sediment samples were freeze-dried and pre-treated with 1 N HCl to remove carbonates. The TOC and $\delta^{13}\text{C}_{\text{org}}$ in surface sediments were analyzed using the same method and equipment as the membrane samples, performed at the Key Laboratory of Submarine Geosciences (KLSG), Ministry of Natural Resources, Hangzhou, China. The reproducibility of TOC (at the 1 σ level) was 0.04 %. The analytical precision of the $\delta^{13}\text{C}_{\text{org}}$ (at the 1 σ level) was about 0.2 %. Sediment samples from core LV77–3 of known TOC content (Astakhov et al., 2020) were analyzed for $\delta^{13}\text{C}_{\text{org}}$ using Picarro G2121 carbon isotopic analyzer. In the process of sample measurement, in order to ensure the stability of the instrument and the accuracy of the $\delta^{13}\text{C}$ value, the standard IAEA-CH3 ($\delta^{13}\text{C} = -24.724$ ‰) was inserted every 10 samples for single point correction. The analytical precision of the $\delta^{13}\text{C}_{\text{org}}$ (at the 1 σ level) was about 0.3 %.

A total of six SPM samples from five sites with different water depths were performed for microstructure analysis using Zeiss Ultra 55 field-emission scanning electron microscope (SEM) equipped with an X-Max 20 EDS system (Oxford Instruments) at the KLSG, with an accelerating voltage of 20 kV. In addition, 16 surface-sediment samples were freeze-dried and sent to the Beta Analytic Laboratory, US, for the $\Delta^{14}\text{C}_{\text{org}}$ analysis.

4. Results

4.1. Particle concentration and composition in the water column

4.1.1. Suspended particulate matter

The SPM concentrations are mostly less than 2.0 mg/L in the surface water (Fig. 2a; Yu et al., 2023). The high concentrations distribute at the northern Bering slope and in the Canada Basin, reaching 6.6 and 9.9 mg/L, respectively. At the Bering Strait entrance and waters north of Alaska, the SPM also comes with the highs of >2.0 mg/L. In comparison, the Chukchi Sea has distinctly low SPM concentrations ranging from 0.1 to 1.9 mg/L.

On both the Bering and Chukchi shelf the SPM concentrations of >4.0 mg/L mainly occur in waters deeper than 10 m (Fig. 2a; Yu et al., 2023). The highest value of 10.3 mg/L occurs at a water depth of 50 m at the Bering Strait entrance. Along with the Bering Strait inflow, high SPM concentrations (> 4.0 mg/L) in the Chukchi Sea are confined to the bottom waters. In contrast, low concentrations (mostly <2.0 mg/L) characterize waters deeper than 10 m in the Canada Basin. Still, the average concentrations in the Canada Basin are an order of magnitude higher than in the Bering Sea.

4.1.2. Particulate OC

Regional concentrations of POC in the surface water show considerable variability (Fig. 2b; Yu et al., 2023). The Chukchi Sea has generally low POC concentrations of <0.1 mg/L. Higher concentrations of >0.1 mg/L mainly occur in the Canada Basin and the Beaufort Sea, with a maximum of 0.4 mg/L. Medium values, from 0.1 to 0.2 mg/L, characterize the northern Bering Sea between St. Lawrence Island and the Bering Strait.

The POC appears to be enriched mainly in the upper 10 m of the water column, with an average concentrations here at least five times higher than in deeper waters (Fig. 2b; Yu et al., 2023). In the central Canada Basin and near the Beaufort Shelf, high concentrations (> 0.1 mg/L) occur only in the surface water. The Bering Strait is different as the POC here is distributed more evenly through the entire water column, with highs of >0.1 mg/L.

4.1.3. $\delta^{13}\text{C}_{\text{org}}$

The highest $\delta^{13}\text{C}_{\text{org}}$ values in the surface water (> –25.0 ‰) characterize the area around the Bering Strait (Fig. 2c; Yu et al., 2023). In most of the northern Bering Sea $\delta^{13}\text{C}_{\text{org}}$ is less than –27.0 ‰. Distinctly low values also occur in the Canada Basin, with the lowest value of –28.7 ‰.

The $\delta^{13}\text{C}_{\text{org}}$ composition in the Bering and Chukchi seas shows a trend similar to the SPM concentration, increasing with water depth (Fig. 2c; Yu et al., 2023). The values of > –24.0 ‰ are mainly concentrated in the bottom water, with a maximum of –19.6 ‰ at a depth of 20 m in the Bering Strait. However, at stations covered by sea ice north of 77°N, the $\delta^{13}\text{C}_{\text{org}}$ reaches the lowest value of –33.4 ‰ in the upper halocline, at a water depth of ~50 m. Another 16 samples in the Canada Basin with the $\delta^{13}\text{C}_{\text{org}}$ ranging from –30.2 to –32.9 ‰ are recovered from depths between 20 and 50 m.

4.1.4. Electron microscopy

Diatoms dominate biogenic particles in the SPM, accompanied by abundant terrestrial debris (Fig. 3). Planktonic foraminifer *Globigerinita* sp. with a diameter of ~100 μm occasionally appears at a water depth of

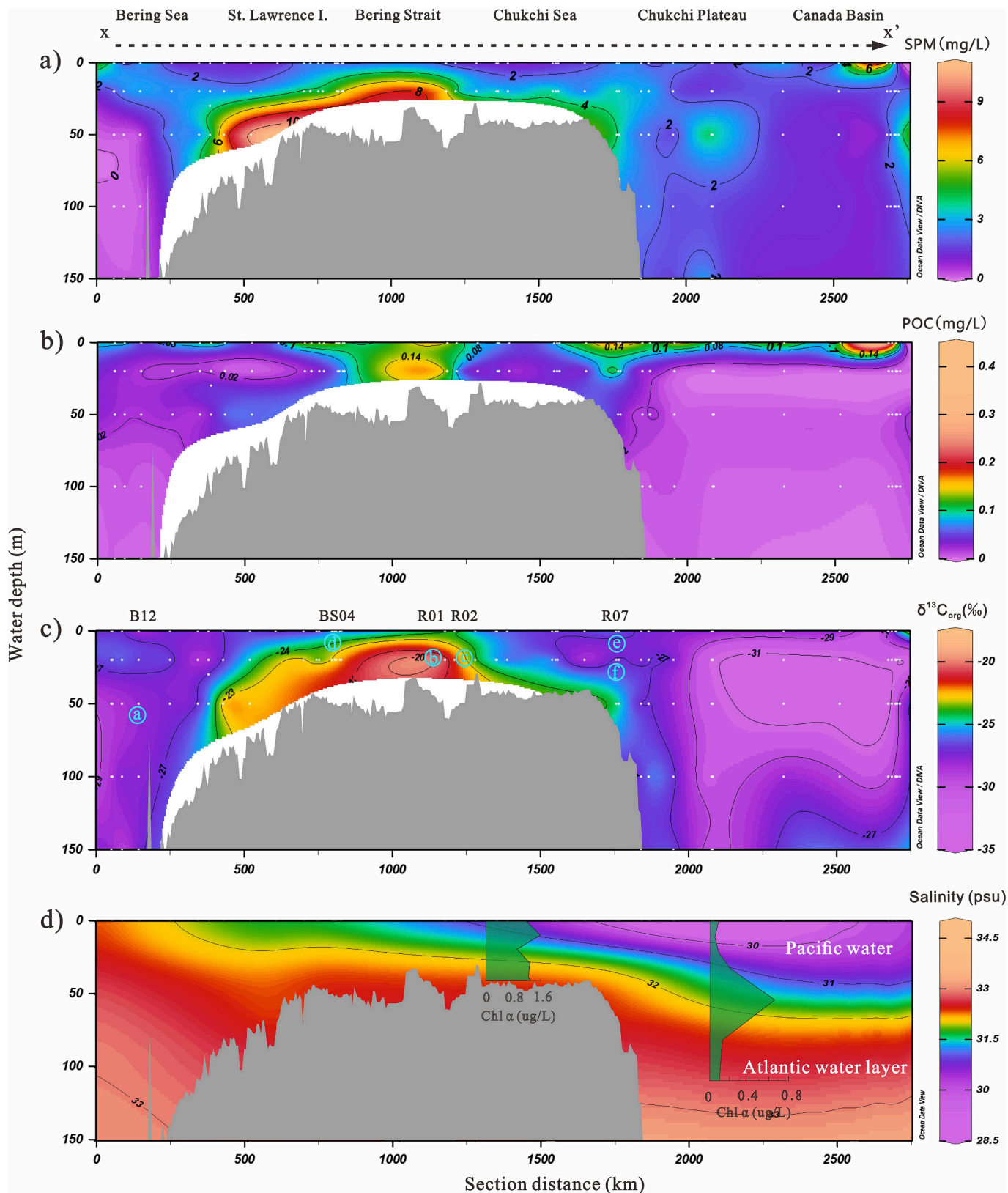
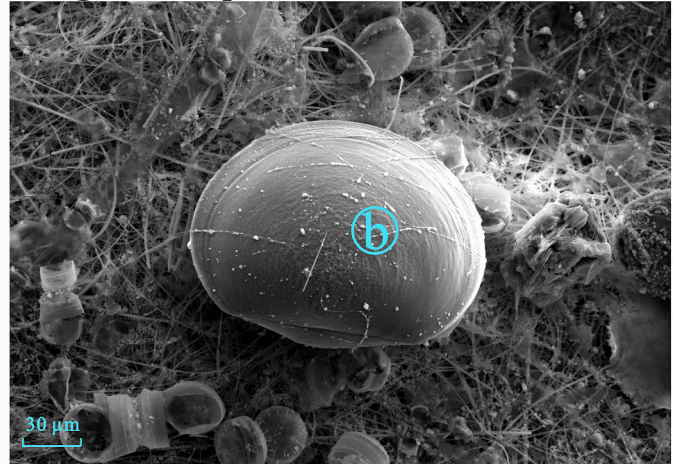


Fig. 2. SPM in the water depth profile from the Bering Sea to the Canada Basin. a) SPM concentration, b) POC concentration, c) PC- $\delta^{13}C_{org}$, and d) Upper water structure. White dots represent SPM sampling layers at different water depths. Cyan-blue letters with circles indicate sampling sites for scanning electron microscopy (Fig. 3). The translucent green shadow in the first profile on the left indicates the distribution of chlorophyll in the Chukchi Sea and the deep basin (Li et al., 2017). Salinity data is from (Zweng et al., 2019). (For interpretation of the references to colour in this figure legend, the reader is referred to the web version of this article.)

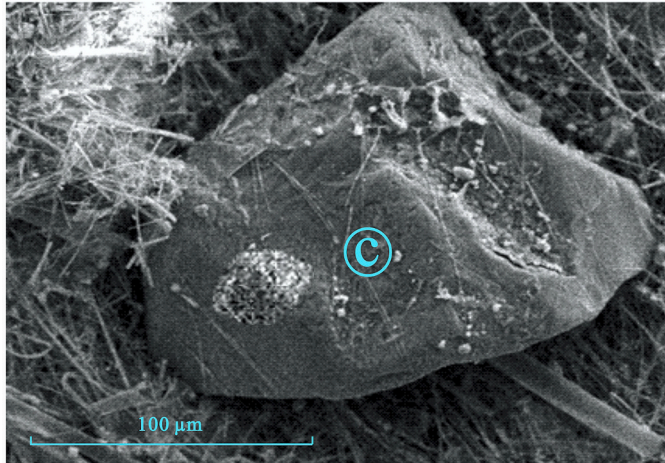
B12@water depth=50 m



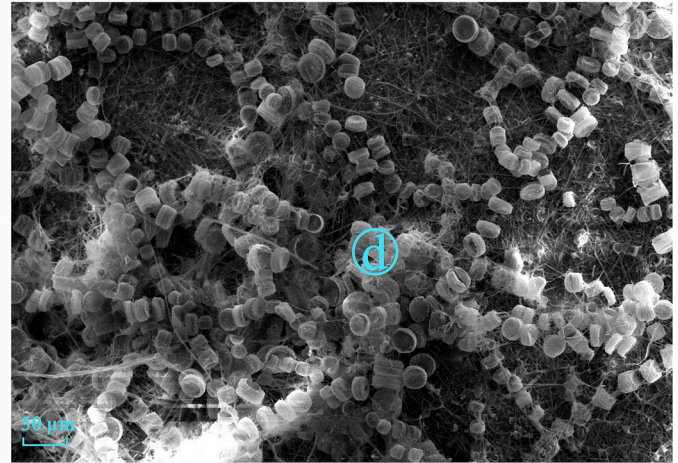
R01@water depth=20 m



R02@water depth=20 m



BS04@water depth=0 m



R07@water depth=0 m



R07@water depth=20 m

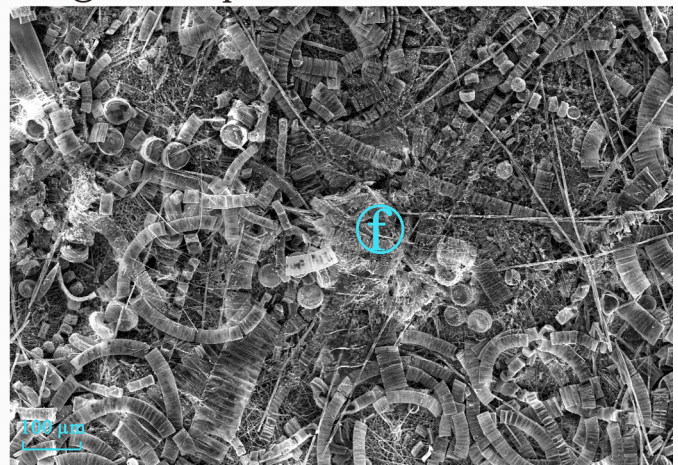


Fig. 3. Electron microscopy of bio/lithogenic SPM typical for different sites. a) Foraminifer *Globigerinita* sp. at the water depth of 50 m for site B12. b) Bivalve shell at the water depth of 20 m for site R01. c) Quartz grain at the water depth of 20 m for site R02. d) Diatom *Thalassiosira* sp. with a visible chain structure at the water depth of 0 m for site BS04. e) and f) Diatom *Fragilariopsis* sp. with a visible chain structure at the water depth of 0 m and 20 m for site R07.

50 m in the Bering Sea. Bivalves with a diameter of ~150 μm are frequent in a sample from water depth of 20 m in the Bering Strait. Quartz particles with a diameter of ~200 μm were found in the same sample.

Diatom *Thalassiosira* sp. dominates biogenic particles from the Bering Sea surface water (Fig. 3). The organic part of the frustules is well preserved, with a visible chain structure. In the Chukchi Sea, the diatom

Fragilariopsis sp. prevails in the surface water and continues to dominate at a larger water depth of 20 m, where diatom abundance is higher. From the morphology perspective, there is no significant difference between the diatoms from the surface water and the 20-m depth.

4.2. Organic carbon composition in sediments

4.2.1. Marine $\delta^{13}\text{C}_{\text{org}}$

The marine $\delta^{13}\text{C}_{\text{org}}$ contribution in surface sediments was derived from correlation between the $\Delta^{14}\text{C}_{\text{org}}$ and $\delta^{13}\text{C}_{\text{org}}$ values (Fig. 4a). For the 22 surface samples, $\Delta^{14}\text{C}_{\text{org}}$ varies from -921 to -171 ‰ (Table 1). The fraction modern (FM), that is the ratio between measured $\Delta^{14}\text{C}_{\text{org}}$ and the 1950 atmospheric $\Delta^{14}\text{C}$, ranges from 8 % to 83 % (Table 1). The patterns of linear relationship between the FM and $\delta^{13}\text{C}_{\text{org}}$ are different for samples from the southern and northern parts of the Chukchi Sea margin (south and north of 73°N) (Fig. 4a). If we assume that all OM is derived from modern marine primary production (i.e., FM = 100 %), the corresponding $\delta^{13}\text{C}_{\text{org}}$ values for these two groups of -19.8 ± 0.3 ‰ and -16.0 ± 0.4 ‰, respectively, would represent marine $\delta^{13}\text{C}_{\text{org}}$ in bulk sediment (Fig. 4a; Blattmann et al., 2018). We hereby use these values as new marine $\delta^{13}\text{C}_{\text{org}}$ EMs for the study areas south and north of 73°N , respectively.

4.2.2. Net $\delta^{13}\text{C}_{\text{org}}$

In a simple two-EM mixing model with terrestrial and marine $\delta^{13}\text{C}_{\text{org}}$ EMs, the slope of a plot for TOC versus $\text{TOC} \times \delta^{13}\text{C}_{\text{org}}$ reflects the net isotopic value of the OC added or removed as terrestrial and marine contributions to TOC changes (Fig. 5b; Aller and Blair, 2006; Aller et al., 2008; Coffin et al., 2017). Strong linear regressions with different slopes were obtained for samples from several sediment cores south of 73°N , surface sediments north of 73°N , and the SPM (Fig. 4b). Samples from cores LV77–3, 05JPC, and PC1 show the slopes of -19.2 ‰, -20.0 ‰, and -20.2 ‰, respectively, close to the surface sediments (-21.4 ‰) but much heavier than in the SPM (-26.8 ‰). Based on the new marine $\delta^{13}\text{C}_{\text{org}}$ EM described above, the marine contribution to TOC changes can be estimated up to nearly 100 %, 97 %, and 94 % through vertical sediment cores LV77–3, 05JPC, and PC1, respectively. In comparison, the average marine contribution is near zero in the SPM, and becomes ~ 50 % in surface sediments north of 73°N .

4.2.3. Riverine new carbon

The riverine new carbon values estimated in a three-EM mixing model for surface sediment samples from the southern Chukchi shelf (south of 73°N) comprise 1–17 % of the TOC (Table 1; Fig. 5a). After excluding the proportion of marine OC, the riverine new carbon accounted for ~ 25 % of the terrestrial OC. In contrast, the negative solution of the mass balance equation in the mixing model indicates that riverine new carbon is no longer present in surface sediment from the northern Chukchi Sea margin (Table 1).

4.2.4. Terrestrial OC

Since the riverine new carbon survives neither sediment burial nor distant transport (surface sediments north of 73°N), we simplified the three-EM mixing model to just two EMs: marine and terrestrial. The model comparison is provided by thirteen surface-sediment samples south of 73°N . The marine fraction estimates by the two- and three-EM mixing model are very similar, with an average standard deviation of 2.7 %, and the terrestrial fraction is equivalent to the sum of riverine and coastal erosion contributions (Table 1).

The terrestrial fraction dominates the Canada Basin and the coastal zone, where it exceeds 60 % (Fig. 5a). This fraction is usually less than 40 % on the shelf, and the low numbers of <20 % characterize the area around the Bering Strait. In terms of TOC, the terrestrial-OC content in bulk sediment has a more complex distribution. Except for sediments in the Canada Basin and on the Beaufort Shelf, generally enriched in terrestrial OC, high values of >0.6 % also occur within and in front of the Herald and Barrow canyons (Fig. 5b). The low values of <0.4 % are widely distributed on the Bering and Chukchi shelves in water depths of <50 m.

In Core LV77–3 from the Herald Canyon head, the terrestrial-OC content shows a general increase with burial time, rising from 0.5 % in the late Holocene to 1.1 % by the middle Holocene, around 5 ka. Superimposed on this trend are lower-amplitude, higher-frequency fluctuations (Fig. 6). An even longer-term increase from 0.5 % to 0.9 % is observed in Core 05JPC from the Barrow Canyon mouth, although there is an apparent decrease in terrestrial-OC content during the early

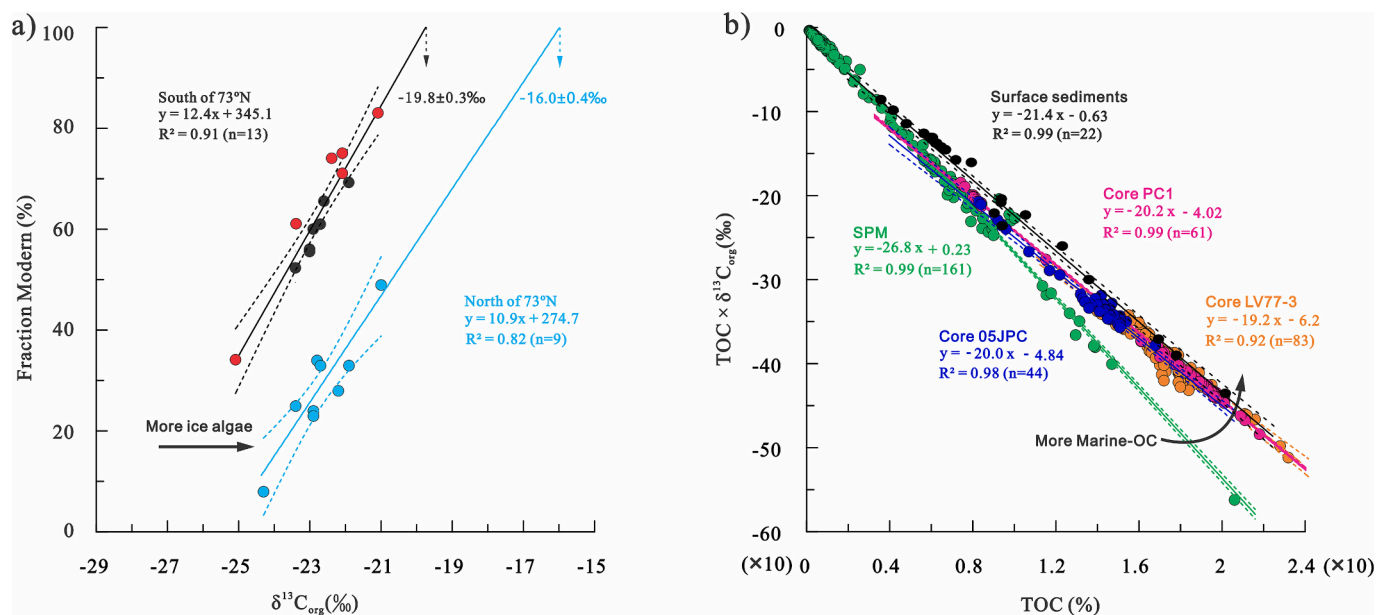


Fig. 4. Linear relationships for $\delta^{13}\text{C}_{\text{org}}$ vs. Fraction Modern (FM) and TOC vs. $\text{TOC} \times \delta^{13}\text{C}_{\text{org}}$ with 95 % confidence intervals shown by dashed lines. a) Relationships between $\delta^{13}\text{C}_{\text{org}}$ and FM in sediments south of 73°N (black) and north of 73°N (blue) with solutions of -19.8 ± 0.3 ‰ and -16.0 ± 0.4 ‰, respectively, given an FM of 100 %. Red dots indicate data from Circum-Arctic Sediment Carbon Database (CASCADE) (Martens et al., 2021). b) Relationships between TOC and $\text{TOC} \times \delta^{13}\text{C}_{\text{org}}$ in the SPM (green), surface sediments north of 73°N (black), core PC1 (magenta), core 05JPC (blue), and core LV77–3 (khaki), with slopes of -26.8 ‰, -21.4 ‰, -20.2 ‰, -20.0 ‰, and -19.2 ‰, respectively. (For interpretation of the references to colour in this figure legend, the reader is referred to the web version of this article.)

Table 1

Organic carbon composition in surface sediments estimated using the two- and three-EM mixing model (details in Supplementary Tex. S1). The dashed-line separates samples south and north of 73°N (asterisks mark the southern sites). Data for surface sediment stations UTN7, CEN1A, HC-2, HC-26, BC6, and PC1–1 (4-PC1) are from CASCADE (Martens et al., 2021), respectively.

No.	Station	Lon. (°W)	Lat. (°N)	$\delta^{13}\text{C}_{\text{org}}$ (‰)	$\Delta^{14}\text{C}_{\text{org}}$ (‰)	FM (%)	2-EMs model (% $\pm\sigma$)		3-EMs model (% $\pm\sigma$)		
							Marine	Terrestrial	Marine	Riverine	Coastal erosion
1	*R02	169.022	67.681	-21.9	-306	69	71 \pm 3	29 \pm 3	68 \pm 2	4 \pm 3	27 \pm 2
2	*UTN7	168.933	68.000	-21.1	-171	83	82 \pm 2	18 \pm 2	81 \pm 2	7 \pm 3	12 \pm 1
3	*R04	168.879	68.201	-22.6	-343	66	62 \pm 3	38 \pm 3	58 \pm 2	11 \pm 3	31 \pm 2
4	*C01	168.161	69.227	-22.9	-398	60	58 \pm 4	42 \pm 4	53 \pm 3	10 \pm 3	37 \pm 2
5	*CEN1A	178.299	70.709	-23.4	-389	61	51 \pm 4	49 \pm 4	47 \pm 3	17 \pm 4	36 \pm 3
6	*C05	164.742	70.769	-23.0	-438	56	56 \pm 4	44 \pm 4	51 \pm 3	7 \pm 4	42 \pm 2
7	*HC-2	175.013	70.900	-22.1	-246	75	68 \pm 3	32 \pm 3	66 \pm 2	14 \pm 3	20 \pm 2
8	*R08	168.858	71.177	-23.4	-475	52	51 \pm 4	49 \pm 4	46 \pm 3	9 \pm 4	45 \pm 2
9	*HC-26	174.395	71.788	-22.1	-287	71	68 \pm 3	32 \pm 3	65 \pm 2	10 \pm 3	25 \pm 2
10	*BC6	154.037	72.233	-25.1	-659	34	27 \pm 6	73 \pm 6	20 \pm 4	15 \pm 5	65 \pm 3
11	*S11	161.486	72.438	-23.0	-443	56	56 \pm 4	44 \pm 4	52 \pm 3	6 \pm 4	42 \pm 2
12	*R10	168.796	72.836	-22.7	-388	61	60 \pm 3	40 \pm 3	56 \pm 2	8 \pm 3	36 \pm 2
13	*PC1–1	175.727	72.839	-22.4	-259	74	64 \pm 3	36 \pm 3	62 \pm 2	17 \pm 3	21 \pm 2
14	E21	179.755	75.154	-21.0	-509	49	55 \pm 3	45 \pm 3	51 \pm 2	-2 \pm 3	51 \pm 2
15	16R13	169.099	75.445	-22.8	-657	34	39 \pm 3	61 \pm 3	34 \pm 3	-0.5 \pm 4	67 \pm 3
16	P23	161.228	76.323	-22.7	-666	33	40 \pm 3	60 \pm 3	35 \pm 3	-3 \pm 4	68 \pm 3
17	R16	168.964	77.079	-22.9	-756	24	38 \pm 3	62 \pm 3	32 \pm 3	-11 \pm 5	79 \pm 4
18	E24	179.836	77.876	-22.2	-724	28	44 \pm 3	56 \pm 3	39 \pm 3	-15 \pm 5	76 \pm 4
19	R17	169.143	78.028	-21.9	-668	33	47 \pm 3	53 \pm 3	42 \pm 3	-11 \pm 5	69 \pm 4
20	P11	165.932	78.485	-23.4	-750	25	33 \pm 4	67 \pm 4	28 \pm 3	-5 \pm 5	77 \pm 4
21	R20	168.543	80.639	-24.3	-921	8	25 \pm 4	75 \pm 4	18 \pm 4	-16 \pm 6	98 \pm 5
22	R13–1	162.223	77.800	-22.9	-771	23	38 \pm 3	62 \pm 3	32 \pm 3	-13 \pm 5	81 \pm 4

Holocene, around 8–9.5 ka (Fig. 6). In the late Holocene sediments of Core PC1 from the Herald Canyon mouth, the terrestrial-OC content ranges from 0.5 % to 0.8 %, with a slight increase downcore. However, a clear long-term trend cannot be identified due to a large hiatus in the middle Holocene, below approximately 3.5 ka (Fig. 6).

4.2.5. Marine OC

The two-EM mixing model shows that the marine OC dominates the shelves, with the marine fraction generally exceeding 60 % (Fig. 5c). The highest values of >90 % mainly occur in the northern Bering Sea between the St. Lawrence Island and the Bering Strait. In the Canada Basin and the coastal zone, the marine fraction is significantly reduced to <40 %. The distribution of marine-OC content in bulk sediment is somewhat different. A large amount of marine OC is concentrated in the canyons with the contents of >1 % (Fig. 5d). Like terrestrial OC, the marine-OC content is also low (<0.5 %) on the Bering and Chukchi shelves in water depths of <50 m. Notably, in the northern Bering Sea, where the marine fraction exceeds 90 %, the marine-OC content is less than 0.5 %. A very low content of <0.25 % is typical for the central Canada Basin.

In core LV77–3, the marine-OC content generally decreases from 1.6 % in the late Holocene to 0.6 % in the middle Holocene, while terrestrial-OC content increases by 0.6 % (Fig. 6). Furthermore, the marine OC curve has prominent second-order peaks apparently in opposition to those of the terrestrial OC. A long-term decreasing trend in marine OC from 1 % to 0.2 % appears in core 05JPC, but without pronounced second-order peaks (Fig. 6). In core PC1, the marine OC also decreases from 1.4 % in the late Holocene to 0.8 % in the middle Holocene above the hiatus.

5. Discussion

5.1. Separation of marine and terrestrial particles

Our observations, augmented by the data from Bates et al. (2005), Goñi et al. (2021), and Xiang and Lam (2020), allow us to evaluate the relationship between particle distribution and hydrodynamics (Fig. 2). The most abundant SPM on the shelf is found between St. Lawrence Island and the Bering Strait, which is consistent with the intense

hydrodynamics in shallow areas (Fig. 2a; Abe et al., 2019; Xiang and Lam, 2020). In open waters, particles undergo mechanical separation due to the competing forces of buoyancy and gravity (Yan and Koplak, 2009). Fine particles (finer than ~50 μm) are easily suspended and constitute the main SPM component, whereas coarser particles are sparsely scattered in the water column (Fig. 3; Xiang and Lam, 2020). After Pacific water enters the Chukchi Sea, the weakening hydrodynamics lead to the release and deposition of particles, both fine and coarse, resulting in a paucity of SPM in the surface waters (Fig. 2a; Abe et al., 2019; Kolesnik et al., 2017; Woodgate, 2018). Based on samples collected in open waters (south of 77° N), a small number of fine particles enter the deep basin within the upper 10 m of water, primarily along cross-shelf canyons such as the Barrow Canyon (Fig. 2a; Bates et al., 2005; Goñi et al., 2021; Xiang and Lam, 2020). Another, possibly more significant transportation factor is the sea ice formed on the shallow shelf. Although the Laptev and East Siberian seas are considered the primary sources of modern Arctic sea ice (e.g., Nürnberg et al., 1994), the Chukchi and Beaufort seas also contribute large volumes of sediment-laden sea ice, potentially increasing in the warming climate (Darby et al., 2009; Eicken et al., 2005).

The POC distribution confirms that most of the SPM concentrated in the shelf bottom water is inorganic debris, while the SPM in the upper 10 m of water contains at least five times more OC than the underlying waters (Fig. 2b). This high POC level can be attributed to both terrestrial input and relatively high marine primary production in the Chukchi Sea (Li et al., 2017; Stabeno et al., 2020; Yunker et al., 2011). The distribution of $\delta^{13}\text{C}_{\text{org}}$ provides further insight into the OC source (Fig. 2c). According to the previously reported average $\delta^{13}\text{C}_{\text{org}}$ for regional marine and terrestrial OC in open waters (Martens et al., 2019), terrestrial OC should dominate the POC in the upper 10 m of water (Fig. 3c). Terrestrial OC is mainly adsorbed by clay minerals or associated with fine particles, making it easily suspended, entrained in ice, and transported (Belicka et al., 2004b; Nürnberg et al., 1994; Ransom et al., 1998). In contrast, marine OC dominates waters deeper than 10 m on the Bering and Chukchi shelves. Biogenic particles in shallow, high-latitude environments sink as chains or aggregates that do not fully degrade before reaching the seafloor, thereby supporting high export rates (Belicka et al., 2004b; O'Daly et al., 2020). Electron microscopy images of SPM

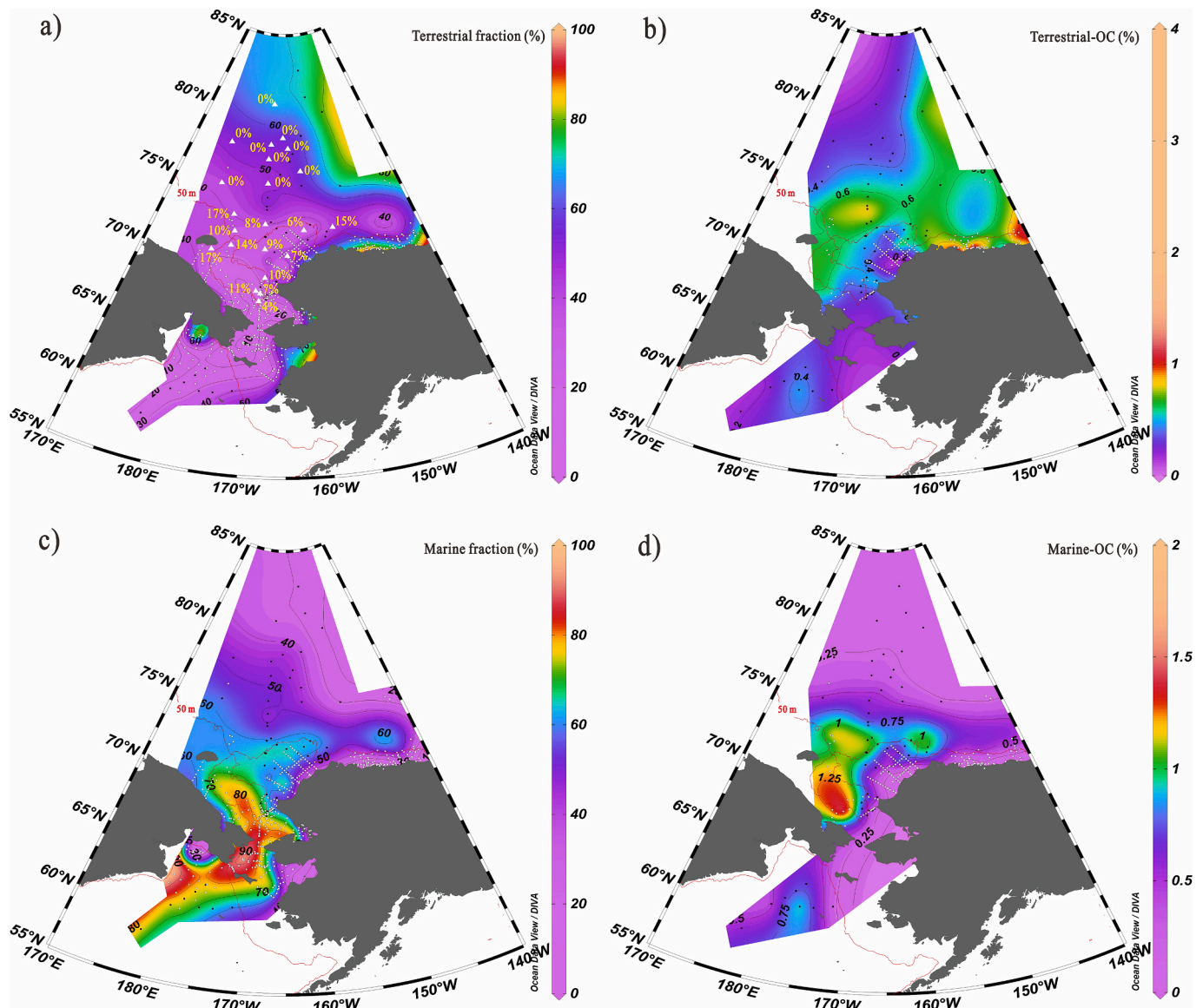


Fig. 5. Organic carbon composition in surface sediments estimated using the 2-EM mixing model. a) Terrestrial organic carbon fraction; overlaid white triangles with yellow numbers indicate the riverine new carbon fraction. b) Terrestrial organic carbon content in bulk sediment. c) Marine organic carbon fraction. d) Marine organic carbon content in bulk sediment. Red thin lines represent 50-m isobaths. Black dots represent 56 samples analyzed in this study. White dots represent 503 data points from Astakhov et al. (2019), Grebmeier and Cooper (2019), Martens et al. (2021), and Naidu et al. (2000). (For interpretation of the references to colour in this figure legend, the reader is referred to the web version of this article.)

demonstrate the visible microalgal chain structures with well-preserved organic parts of the biogenic particles bound to the skeleton (Fig. 3). This morphology may accelerate the settling rates of biogenic particles, leading to their deposition mainly on the shelf (Fig. 2; Buesseler, 1998).

Unlike the $\delta^{13}\text{C}_{\text{org}}$ distribution in shelf waters, the extremely depleted $\delta^{13}\text{C}_{\text{org}}$ values of $< -31.0\text{‰}$ characterize the subsurface water (upper halocline) in the Canada Basin (Fig. 2). Such depleted $\delta^{13}\text{C}_{\text{org}}$ values have also been observed in previous studies (Xiang and Lam, 2020). Although some terrestrial compounds, such as alkanes, have similar isotopic compositions, riverine or coastal POC has been excluded as a direct influence on the extremely depleted $\delta^{13}\text{C}_{\text{org}}$ due to the lack of significant correlation between POC- $\delta^{13}\text{C}_{\text{org}}$ and the fraction of meteoric water/sea ice melt (Drenzek et al., 2007; Brown et al., 2014; Xiang and Lam, 2020). Our data show that extremely depleted $\delta^{13}\text{C}_{\text{org}}$ values only appear in areas covered by perennial sea ice and with strong halocline and nutricline (Fig. 1; Fig. 2). Nutrient supply and photosynthetically active radiation in subsurface waters are greatly limited, thus restricting

phytoplankton growth rates (Laney et al., 2017; Li et al., 2017). Simultaneously, the solubility pump (physical and chemical processes that govern the dissolution and transport of CO_2 in the ocean) is very efficient in the Arctic's low-temperature water, quickly increasing the partial pressure of CO_2 in the mixed layer to approximately $400\ \mu\text{atm}$ (Cai et al., 2010). Aqueous CO_2 has a lighter $\delta^{13}\text{C}$ (approximately -12.0‰ to -8.0‰) than bicarbonate (approximately 0.0‰ to 2.0‰) (Zeebe and Wolf-Gladrow, 2001; Close, 2019). Assuming a classic isotope fractionation of -24.0‰ between aqueous CO_2 and phytoplankton, and without an efficient biogenic pump (biological processes that transport carbon from the surface ocean to the deep ocean), as in the subsurface water in the Canada Basin, high partial pressure of CO_2 will result in extremely depleted $\delta^{13}\text{C}_{\text{org}}$ of phytoplankton (Alling et al., 2012; Stein and Macdonald, 2004; Xiang and Lam, 2020). Therefore, the highly depleted $\delta^{13}\text{C}_{\text{org}}$ indicates that marine and terrestrial OC are enriched in different water layers in the Canada Basin, and importantly, the marine OC on the Chukchi Shelf has not been transported laterally into the deep

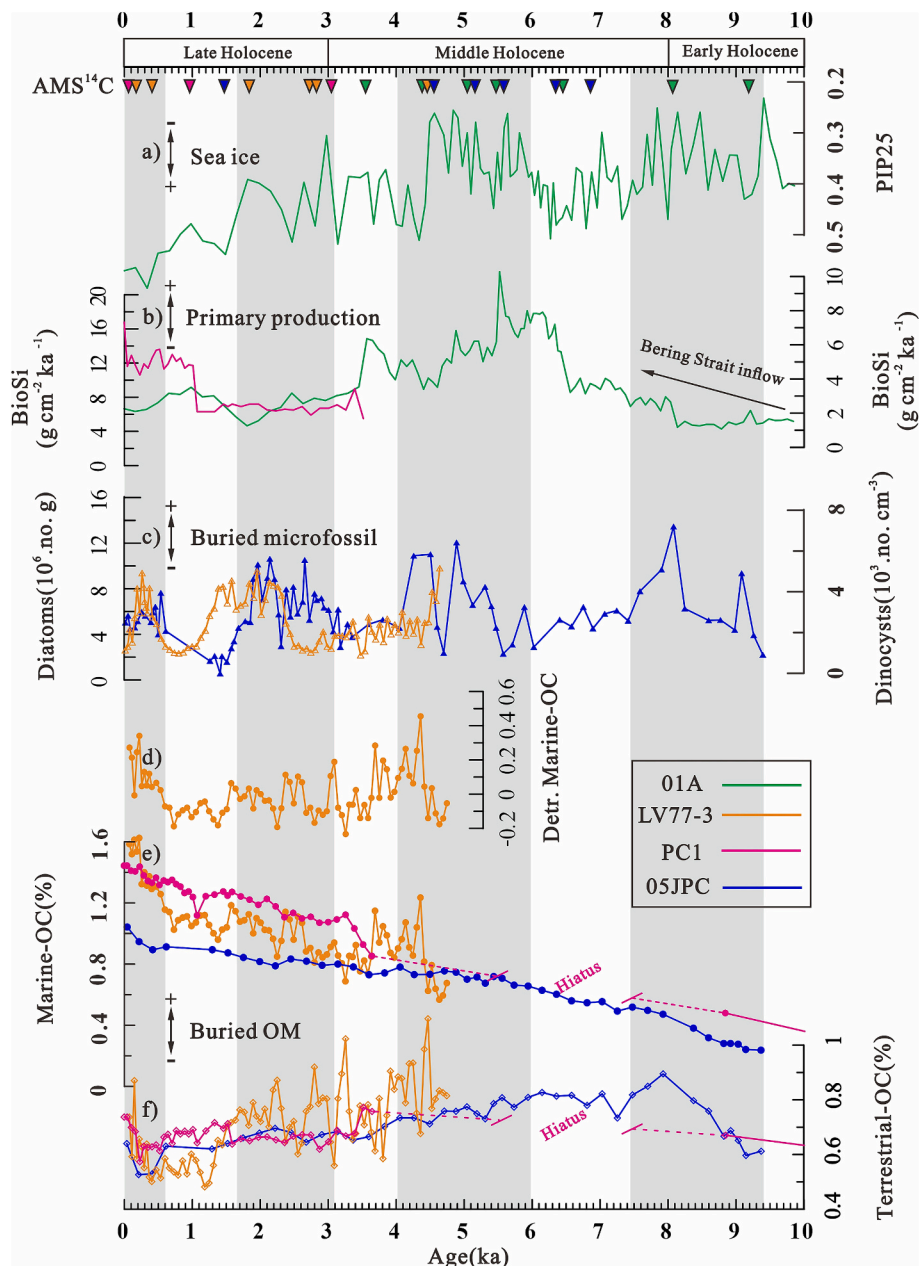


Fig. 6. Downcore records of OC content and marine production proxies. Top to down: ice algae proxy PIP25 in core 01 A (Stein et al., 2017) (a); Bio-silicon fluxes (cores 01 A and PC1) (Stein et al., 2017; Swärd et al., 2018) (b); diatom and dinocyst abundances (cores LV77-3 and 5JPC) (Astakhov et al., 2020; McKay et al., 2008) (c); detrended marine OM in core LV77-3 (d); marine and terrestrial OM content (cores LV77-3, PC1 and 5JPC) (e and f). Sediment cores are colour-coded. Intervals with higher production are shaded.

basin in large quantities.

Overall, the SPM data show different transport patterns for marine and terrestrial OC. This difference indicates the separation of marine and terrestrial particles in the surface/subsurface waters, resulting from differential hydrodynamics, transportation agents, phytoplankton communities, and particle morphology. As a result of differential transport, the OC was preferentially buried in marine or terrestrial components in different areas (Fig. 7).

5.2. Organic carbon deposition and degradation

5.2.1. Ice algae OC contribution

A linear regression between the TOC and $\text{TOC} \times \delta^{13}\text{C}_{\text{org}}$ in surface sediments north of 73°N has a slope of -21.4‰ (Fig. 4b), representing the net $\delta^{13}\text{C}_{\text{org}}$ of the deposited OC (Aller and Blair, 2006; Coffin et al.,

2017). Since the measured net $\delta^{13}\text{C}_{\text{org}}$ of the SPM in the study area is -26.8‰ (Fig. 4b), it is evident that the suspended OC collected in July–August does not fully represent the deposited OC. Given a -21.0‰ $\delta^{13}\text{C}_{\text{org}}$ value of the marine EM in the mixing model of Martens et al. (2019), nearly 93 % of the OC in sediments north of 73°N must be derived from marine primary production. However, based on biomarkers, the fraction of marine OC off the Chukchi Shelf is less than 54 % (Belicka and Harvey, 2009). Simultaneously, $\delta^{13}\text{C}_{\text{org}}$ values of $> -21.0\text{‰}$ frequently occur in the surface sediments of the Bering Shelf and the Canada Basin (Naidu et al., 2000). Therefore, there must be a substantial amount of unaccounted ^{13}C -rich organic components deposited on both the shelf and basin seafloor, not in July–August.

Hydrolysis and bacterial production in sediments can lead to ^{13}C enrichment, but the fractionation effect is usually less than 1.0‰ (Close, 2019; Cooper et al., 2015). Another common mechanism is organic

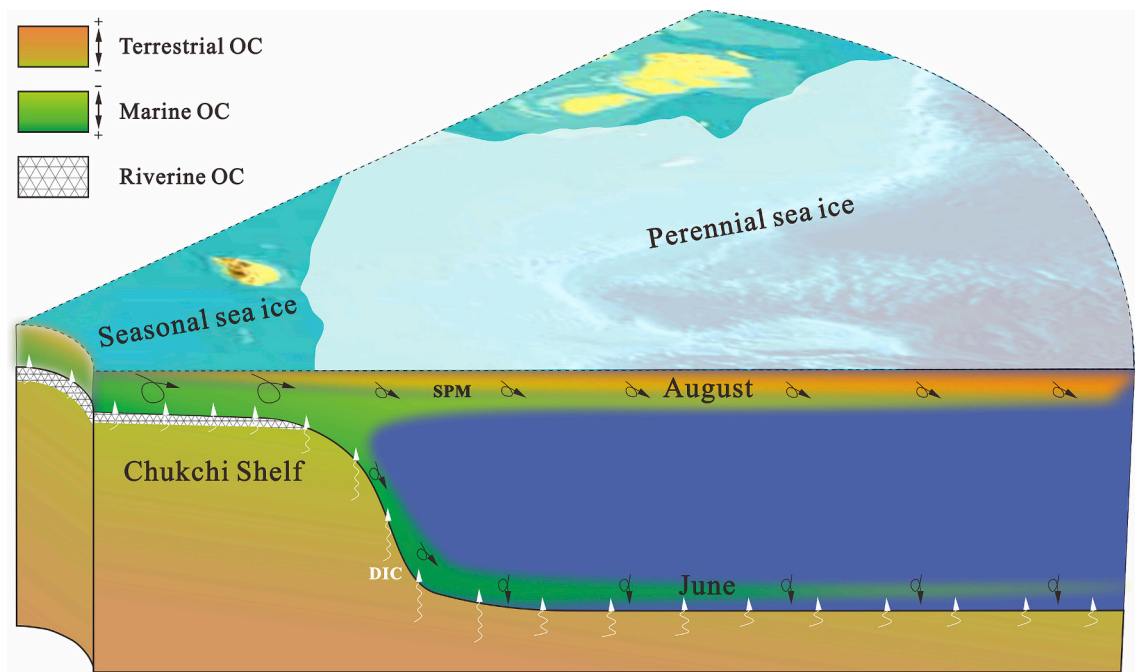


Fig. 7. Chukchi Shelf margin organic carbon burial model. SPM and black curve lines indicate organic carbon lateral transport and differential deposition. DIC (Dissolved Inorganic Carbon) and white curve lines indicate inorganic carbon release due to early-stage diagenesis. August and June represent phytoplankton blooms in different months (Clement Kinney et al., 2020). White translucent area represents perennial sea ice for the 30-year average (1981–2010) (Melsheimer and Spreen, 2019).

carbon degradation, whether microbial or photo degradation, which preferentially breaks ^{12}C chemical bonds, resulting in residual organic carbon being enriched in ^{13}C (Sarkar et al., 2024; Søreide et al., 2006). Unfortunately, the extent of ^{13}C enrichment due to degradation processes in the study area remains unknown. Based on modern observations (Clement Kinney et al., 2020; Stabeno et al., 2020), we believe that a more likely explanation for heavier $\delta^{13}\text{C}_{\text{org}}$ values is related to the input of ice algae. By limiting the exchange of CO_2 between the atmosphere and seawater, sea ice can cause ice algae to thrive in melt ponds and beneath sea ice, resulting in extremely enriched $\delta^{13}\text{C}_{\text{org}}$ (Close, 2019; Schubert and Calvert, 2001; Stabeno et al., 2020). Modern observations show that primary production can be significantly high not only in ice-free conditions but also under thinning sea ice (Boetius et al., 2013). The percentage of under-ice production was found to be highest in the Northern Chukchi Sea, with 63 % occurring in waters covered by $\geq 50\%$ sea ice and 52.3 % in waters covered by $\geq 75\%$ sea ice, peaking in June, before the major terrestrial OC inputs (Clement Kinney et al., 2020; Stabeno et al., 2020). The contribution of ice algae to sedimentary Arctic Ocean OC with $\delta^{13}\text{C}_{\text{org}}$ values as heavy as -15% to -8% can thus be considerably more significant than initially thought (Arrigo et al., 2014; Stein and Macdonald, 2004). The marine $\delta^{13}\text{C}_{\text{org}}$ values of -19.8% and -16.0% derived from the paired $\Delta^{14}\text{C}_{\text{org}}$ and $\delta^{13}\text{C}_{\text{org}}$ measurements for the study areas south and north of 73°N , respectively (Fig. 4a), not only provide more accurate marine $\delta^{13}\text{C}_{\text{org}}$ EM for the mixed model but also help quantify the contribution of ice algae to sedimentary OC. The average $\delta^{13}\text{C}_{\text{org}}$ of ice algae and open-marine phytoplankton is approximately -11.5% (median between -15.0% and -8.0%) and -21.0% , respectively (Martens et al., 2019; Stein and Macdonald, 2004). Assuming no influence of degradation processes on the $\delta^{13}\text{C}_{\text{org}}$ in sediments, the fraction of ice algae in the marine OC can be calculated using our mixing model as about 14 % and 55 % in the areas south and north of 73°N , respectively. The latter number is close to the 52.3 % of the observed under-ice production in total primary production (Clement Kinney et al., 2020).

5.2.2. Destination of riverine new carbon

Except for minor contributions from secondary production, such as bacteria, the buried OC is gradually removed from the sediment (Aller et al., 2008; Pearson et al., 2001). Apart from the impact of burrowing organisms in near-surface sediments, the primary cause for OC removal is degradation (Aller et al., 2008; Pirtle-Levy et al., 2009). The degradation of terrestrial OC can cause significant seawater acidification, as observed in the Laptev and East Siberian seas, which receive large inputs of riverine new carbon (POC and DOC) (Semiletov et al., 2016). Compared to OC from coastal erosion, the OC carried by modern Arctic rivers contains more fresh/labile components derived from modern plants and the active soil layer, making it more easily degraded in seawater (Martens et al., 2019; Semiletov et al., 2016). The primary source of the riverine new carbon buried in the Chukchi Shelf is POC from the Yukon River, which has an average age of ~ 3700 years and $\Delta^{14}\text{C}_{\text{org}}$ values between -467% and -253% (Guo and Macdonald, 2006). Given that the $\Delta^{14}\text{C}_{\text{org}}$ of riverine new carbon at the northern Chukchi Shelf margin is $-173 \pm 163\%$ (Martens et al., 2019), it may constitute at least 60 % of the Yukon River POC. According to the three-EM mixing model, the riverine new carbon in our data accounts for $\sim 25\%$ of the terrestrial OC in surface-sediment samples south of 73°N , which is much lower than in the Yukon River (Table 1; Fig. 5a). Considering potential inputs from the East Siberian Sea via the Siberian Coastal Current (Semiletov et al., 2016), the contribution from the Yukon River may be even lower. This comparison suggests that a considerable portion of the riverine new carbon undergoes degradation, dilution, or burial during long-distance transportation.

The mixing model also shows that no detectable riverine new carbon is present in all surface sediments north of 73°N (Table 1; Fig. 5a) despite a high total input of terrestrial OC (Fig. 2; Stein and Macdonald, 2004; Yunker et al., 2011). Two major reasons may explain the absence of riverine new carbon in sediments north of 73°N . First, the new carbon in the Mackenzie River, a primary OC source for the Canadian Basin, accounts for only about 30 % of the POC, which is less than in the Yukon River and thus easier to degrade, dilute, or bury during long-distance transportation (Goñi et al., 2005). Second, the fast settling of ballast

sediment material (inorganic mineral components that are often associated with the organic matter) in the Canada Basin is much less prevalent than on the shelf, where weakening hydrodynamics north of the Bering Strait cause massive SPM deposition that aids better preservation of the riverine new carbon. A similar pattern is observed in the Laptev and East Siberian seas, where riverine new carbon is not strongly degraded in the coastal zone but only on the outer shelf (Semiletov et al., 2016). Consequently, easily suspendable riverine new carbon cannot settle quickly in the Canada Basin but undergoes longer degradation time in the water column (Fig. 7; Belicka et al., 2004a).

5.2.3. Preferential degradation of marine OC in sediments

Degradation of the marine OC is illustrated by a gradual decrease in its content with sediment depth in all three cores analyzed for $\delta^{13}\text{C}_{\text{org}}$ (Fig. 6). Based on the net $\delta^{13}\text{C}_{\text{org}}$ values, the marine contribution to totally removed OC is up to 93 %, 96 %, and nearly 100 % in cores 05JPC, PC1, and LV77–3, respectively. Thus, the degradation of buried OC in the shelf sediments appears to be dominated by marine OC, except for the relatively fast degradation of the riverine new carbon in the southern part of the shelf (Table 1). We note a potential error in the OC fraction estimation caused by shifts in the perennial sea ice front with different marine $\delta^{13}\text{C}_{\text{org}}$ EM (Fig. 4a). While at present this front generally corresponds to 73°N , it could have shifted south- or northwards with changing paleoclimatic conditions, such as in the relatively warm early-middle Holocene (Polyak et al., 2016; Stein et al., 2017). In such cases, more depleted $\delta^{13}\text{C}_{\text{org}}$ values like -21.0 ‰, characteristic of phytoplankton in open waters (Martens et al., 2019), would expand into more northern areas, including the sites of the sediment cores under study. For example, a -21 ‰ $\delta^{13}\text{C}_{\text{org}}$ marine EM for the 4–9 ka record in core 05JPC would result in the estimated marine-OC content being 0.12 % higher than in the current setting (where the marine $\delta^{13}\text{C}_{\text{org}}$ EM is -19.8 ‰). Still, the offset value would not be high enough to change the overall decreasing trend in the downcore marine OC distribution (Fig. 6).

The distinct downcore decrease in the marine OC content is not reflected in other biogeochemical proxies for primary production, including phytoplankton microfossils and ice-algae biomarkers (Fig. 6). This difference indicates that the marine-OC decrease is primarily controlled by degradation rather than depositional factors such as sediment dilution and burial. After 3–4 kyr, the time interval well characterized in all three cores, about 30 % of the marine OC is degraded in cores PC1 and LV77–3, with a lesser amount in the more northerly core 05JPC. The remaining marine OC will likely degrade over a more extended period as degradation rates generally decrease exponentially (Arndt et al., 2013). Considerable variations in the abundances of dinocysts and diatoms in cores 05JPC and LV77–3, respectively, and in the ice algae biomarker PIP25 in core 01 A have been interpreted in relation to changes in sea ice conditions (Fig. 6; Astakhov et al., 2020; McKay et al., 2008; Stein et al., 2017). Generally consistent larger-scale variations in these proxies indicate millennial variability in the Holocene, with several periods of reduced ice cover lasting 1–2 kyr. Superimposed smaller-scale fluctuations presumably correspond to higher-frequency variability. The detrended marine-OC record in core LV77–3 is partially consistent with the diatom variations, at least in the upper part, ~ 2.5 ka (Fig. 6). This pattern corroborates the control of sea ice extent and conditions on the input of marine OC to the sea floor. Nevertheless, these variations do not have a long-term effect on the marine-OC degradation in sediments.

Compared to the OC content in sediments, fluxes of the OC components, as well as related proxies such as biogenic silica (a proxy for marine production), exhibit a different pattern overwhelmingly controlled by the rates of sediment deposition (Fig. 6). At the northern/eastern margin (cores 01 A and 05JPC), the highest linear sedimentation rates (LSR) of up to 250 cm/kyr characterize the middle Holocene, ~ 6.5 – 4.5 ka, whereas in the Herald Canyon, comparable rates were attained only in the last millennium. Both LSR maxima generally

correspond to intervals of reduced sea ice, but their asynchronicity and low rates in other similar intervals indicate that sea ice extent was not the only depositional factor. Enhanced sedimentation in the middle Holocene was likely influenced by the intensified Bering Strait inflow (Liu et al., 2023; Polyak et al., 2016; Yamamoto et al., 2017), while deposition in the Herald Canyon could be related to a change in the current system. Notably, the middle Holocene is absent in core PC1, probably due to winnowing by bottom currents (Swärd et al., 2018). These changes in sedimentation rates clearly impacted OC deposition, as illustrated by fluxes of proxies for both marine production and terrestrial OC in sediment records (Fig. 6). However, the long-term effect of these enhanced depositional events on OC burial and degradation is not apparent.

5.3. Potential future changes

Arctic climate change is subject to considerable uncertainty. While the Arctic is warming at more than triple the global rate due to amplification, the Atlantic meridional overturning circulation and the poleward freshwater transport have the potential to lead to Arctic cooling and sea ice expansion (Caesar et al., 2021; Sohail et al., 2022; Taylor et al., 2021). Assuming that the current warming continues, the thinning sea ice and increasing melt-pond cover may enhance under-ice production and ice algae export, as suggested by a hypothesis and supported by field observations in 2012 when perennial sea ice shrunk to a record minimum extent (Arrigo et al., 2012; Boetius et al., 2013). At the Chukchi Sea margin, the sea ice extent minimum (15 % ice concentration) for the 30-year period (1981–2010) is close to 73°N (Fig. 1; Fig. 7; Melsheimer and Spreen, 2019). In the area south of 73°N , an ice-free period of at least three months each year provides a time window for the bloom of non-ice algae phytoplankton (Lalande et al., 2020). Ice algae account for about 14 % of the buried marine OC, but their flux in the Chukchi Sea can reach $19 \text{ gC/m}^2/\text{yr}$, estimated from a primary production of $166 \text{ gC/m}^2/\text{yr}$ and an export rate of 82 % (Moran et al., 1997; O'Daly et al., 2020). In contrast, the area north of 73°N is usually covered by sea ice for most of the year, with concentrations ranging from 15 % to 100 %, and overall primary production is an order of magnitude lower than that of the Chukchi Sea, ranging from 7 to $28 \text{ gC/m}^2/\text{yr}$ (Boetius et al., 2013; Watanabe et al., 2014). The export rate of ice algae can exceed 85 % at a water depth of about 4300 m in the central Arctic Ocean, while the export rate of phytoplankton-derived OC at a water depth of about 1300 m in the Northwind pelagic basin is about 23 % (Boetius et al., 2013; Watanabe et al., 2014). Although the average contribution of ice algae to marine OC burial in surface sediments north of 73°N is as high as 55 %, the buried ice algae flux is only $5.2 \text{ gC/m}^2/\text{yr}$, estimated from a median primary production of $17.5 \text{ gC/m}^2/\text{yr}$ and a median export rate of 54 %. Since the sea ice conditions north of 73°N will inevitably approach those of the Chukchi Sea with global warming, the relative proportion of ice algae in growing primary production is bound to decrease, and the export rate of marine OC will be significantly lower in deep waters north of 73°N . In other words, more marine OC will be degraded in the water column, and the initial burial efficiency of marine OC will surely decrease with increasing burial rate in the future.

Another negative factor that may strengthen in the future is the increased input of riverine new carbon. As recorded in surface sediments on the Chukchi Shelf, riverine new carbon accounts for approximately 25 % of the buried terrestrial OC (Table 1). Due to robust lateral transport of terrestrial OC, it is likely that more riverine new carbon was imported towards the deep basin north of 73°N and degraded in the water column. With global warming, the burial rate of terrestrial OC at the Chukchi Shelf margin could increase, analogous to the Mid-Holocene when summer temperatures were about 1.5°C higher than today (Fig. 6; Kurek et al., 2009; Stein et al., 2017). However, the proportion of riverine new carbon in terrestrial OC will rise if permafrost thawing continues (Bröder et al., 2020). Increasing ocean currents and seasonal sea ice will facilitate more robust lateral transport of terrestrial OC (Abe

et al., 2019; Eicken et al., 2005), and terrestrial OC that may deposit in floodplains and thermokarst lakes as ice jams will extend to the outer shelf (Overeem et al., 2022). Furthermore, lability is not inherent but a function of the microbial community, organic carbon chemistry, and environmental conditions (Nguyen et al., 2022). The proportion of riverine new carbon, representing the easily degradable components of terrestrial OC, may further increase with microbial populations in a warmer environment. As more riverine new carbon degrades in the water column, the initial burial efficiency is expected to decrease.

6. Conclusions

The high-resolution observations provide detailed insights into the transport and deposition of particulate OC in the northern Bering Sea, Chukchi Sea, and Canada Basin during July–August. Terrestrial and marine OC exhibit pronounced separation in the water column. Easily suspendable terrestrial OC is concentrated in the upper 10 m of water or sea ice and transported laterally into the Canada Basin. In contrast, faster-settling marine OC is less affected by lateral transport, extending up to the shelf margin in bottom waters and rarely entering the deep basin. This differential deposition directly determines that marine OC experiences less degradation in the water column before burial, resulting in a higher initial burial efficiency than terrestrial OC. Another factor favoring the initial burial efficiency of marine OC is the high export rate of under-ice production. Based on the new marine $\delta^{13}\text{C}_{\text{Org}}$ EM (−19.8 ‰ and −16.0 ‰) for the mixing model, ice algae are identified as contributing about 14 % and 55 % of the OC burial in the areas south and north of 73°N, respectively, verifying the significant impact of under-ice production on OC burial and carbon sink in the Arctic Ocean.

A potential threat to the CO_2 sink in the Arctic Ocean is the decreasing initial burial efficiency of marine OC. As the proportion of ice algae in primary production decreases and the OC burial site extends from the shelf margin to the deep basin, more marine OC will be degraded in the water column and released back into the ocean-atmosphere carbon pool. A similar and potentially more severe negative feedback may arise from riverine new carbon in terrestrial OC, which accounts for approximately 25 % of the buried terrestrial OC in surface sediments on the Chukchi Shelf. Since terrestrial OC is more strongly affected by lateral transport than marine OC, more riverine new carbon is expected to be injected into the deep basin and degraded in the water column. The burial dynamics of terrestrial and marine OC in cores at the Chukchi Shelf margin further indicate that the burial efficiency of terrestrial OC will eventually exceed that of marine OC over time. However, at least since the late Holocene, the negative feedback of marine OC degradation on the carbon sink has not been critical, as only about 10 % of buried marine OC has degraded every millennium. Despite these findings, this study was unable to precisely quantify the carbon sink equivalent generated by primary productivity or to assess the temporal trends of this change. Furthermore, the uncertainty in evaluating carbon burial efficiency, particularly due to the extreme ^{13}C enrichment in ice algae and the significant ^{13}C depletion in subsurface phytoplankton, was not adequately estimated. Addressing these uncertainties and gaps will be crucial in future research.

CRedit authorship contribution statement

Liming Ye: Writing – original draft, Funding acquisition, Conceptualization. **Xiaoguo Yu:** Writing – review & editing, Funding acquisition. **Yanguang Liu:** Writing – review & editing, Validation. **Anatolii S. Astakhov:** Writing – review & editing. **Alexander Bosin:** Writing – review & editing, Data curation. **Yeping Bian:** Data curation. **Linshen Dong:** Writing – review & editing. **Weijia Fan:** Methodology, Data curation. **Haili Yang:** Methodology.

Declaration of generative AI and AI-assisted technologies in the writing process

During the preparation of this work the author used DeepL and Grammarly in order to polish the language. After using these tools, the author reviewed and edited the content as needed and takes full responsibility for the content of the publication.

Declaration of competing interest

The authors declare that they have no known competing financial interests or personal relationships that could have appeared to influence the work reported in this paper.

Data availability

Data on organic carbon composition in sediments is available in the Figshare database: <https://doi.org/10.6084/m9.figshare.25902757>. Data on suspended particulate material will be made available upon request.

Acknowledgements

We express our sincere gratitude to the crew members and scientists aboard the RV *Xuelong* and *Akademik M.A. Lavrentyev* for their support during the 6th Chinese National Arctic Research and the “Arctic Silk Way” Russian-Chinese Expeditions. We extend our appreciation to the Chinese Polar Sample Repository for providing the surface sediments. Special recognition is accorded to Polyak L. for his valuable suggestions. We acknowledge the editor and reviewers for their insightful comments that have greatly enhanced the quality of this manuscript. This research was supported by the National Natural Science Foundation of China (Grant No. 42376064; 42176245), the National Key Research and Development Program of China (Grant No. 2023YFF0804600), the Scientific Research Fund of the Second Institute of Oceanography, Ministry of Natural Resources (Grant No. JG1512), and the Chinese Special Project on Arctic Ocean Marine Geology Investigation (Contract No. CHINARE 2012-2017-03-02).

Appendix A. Supplementary data

Supplementary data to this article can be found online at <https://doi.org/10.1016/j.palaeo.2024.112534>.

References

- Abe, H., Sampei, M., Hirawake, T., Waga, H., Nishino, S., Ooki, A., 2019. Sediment-associated phytoplankton release from the seafloor in response to wind-induced barotropic currents in the Bering Strait. *Front. Mar. Sci.* 6, 97.
- Aller, R.C., Blair, N.E., 2006. Carbon remineralization in the Amazon–Guianas tropical mobile mudbelt: a sedimentary incinerator. *Cont. Shelf Res.* 26, 2241–2259.
- Aller, R.C., Blair, N.E., Brunskill, G.J., 2008. Early diagenetic cycling, incineration, and burial of sedimentary organic carbon in the central Gulf of Papua (Papua New Guinea). *J. Geophys. Res.* Earth 113.
- Alling, V., Porcelli, D., Mörth, C.-M., Anderson, L.G., Sanchez-Garcia, L., Gustafsson, Ö., Andersson, P., Humborg, C., 2012. Degradation of terrestrial organic carbon, primary production and out-gassing of CO_2 in the Laptev and East Siberian Seas as inferred from $\delta^{13}\text{C}$ values of DIC. *Geochim. Cosmochim. Acta* 95, 143–159.
- Arguez, A., Durre, I., Applequist, S., Vose, R.S., Squires, M.F., Yin, X., Heim Jr., R.R., Owen, T.W., 2012. NOAA’s 1981–2010 US climate normals: an overview. *Bull. Am. Meteorol. Soc.* 93, 1687–1697.
- Arndt, S., Jørgensen, B.B., LaRowe, D.E., Middelburg, J., Pancost, R., Regnier, P., 2013. Quantifying the degradation of organic matter in marine sediments: a review and synthesis. *Earth Sci. Rev.* 123, 53–86.
- Arrigo, K.R., van Dijken, G., Pabi, S., 2008. Impact of a shrinking Arctic ice cover on marine primary production. *Geophys. Res. Lett.* 35.
- Arrigo, K.R., Perovich, D.K., Pickart, R.S., Brown, Z.W., Van Dijken, G.L., Lowry, K.E., Mills, M.M., Palmer, M.A., Balch, W.M., Bahr, F., 2012. Massive phytoplankton blooms under Arctic Sea ice. *Science* 336, 1408.
- Arrigo, K.R., Perovich, D.K., Pickart, R.S., Brown, Z.W., van Dijken, G.L., Lowry, K.E., Mills, M.M., Palmer, M.A., Balch, W.M., Bates, N.R., 2014. Phytoplankton blooms

- beneath the sea ice in the Chukchi Sea. *Deep-Sea Res. II Top. Stud. Oceanogr.* 105, 1–16.
- Astakhov, A., Gusev, E., Kolesnik, A., Shakirov, R., 2013. Conditions of the accumulation of organic matter and metals in the bottom sediments of the Chukchi Sea. *Russ. Geol. Geophys.* 54, 1056–1070.
- Astakhov, A., Sattarova, V., Xuefa, S., Limin, H., Aksentov, K., Alatorsev, A., Kolesnik, O., Mariash, A., 2019. Distribution and sources of rare earth elements in sediments of the Chukchi and East Siberian Seas. *Polar Sci.* 20, 148–159.
- Astakhov, A., Shi, X., Darin, A., Kalugin, I., Hu, L., Tsoy, I., Kolesnik, A., Obrezkova, M., Alatorsev, A., Babich, V., 2020. Reconstructing ice conditions in the southern Chukchi Sea during the last millennium based on chemical composition of sediments and diatom assemblages. *Mar. Geol.* 427, 106220.
- Bates, N.R., 2006. Air-sea CO₂ fluxes and the continental shelf pump of carbon in the Chukchi Sea adjacent to the Arctic Ocean. *J. Geophys. Res. Oceans* 111.
- Bates, N.R., Hansell, D.A., Moran, S.B., Codispoti, L.A., 2005. Seasonal and spatial distribution of particulate organic matter (POM) in the Chukchi and Beaufort Seas. *Deep-Sea Res. II Top. Stud. Oceanogr.* 52, 3324–3343.
- Belicka, L.L., Harvey, H.R., 2009. The sequestration of terrestrial organic carbon in Arctic Ocean sediments: a comparison of methods and implications for regional carbon budgets. *Geochim. Cosmochim. Acta* 73, 6231–6248.
- Belicka, L.L., Macdonald, R.W., Yunker, M.B., Harvey, H.R., 2004a. The role of depositional regime on carbon transport and preservation in Arctic Ocean sediments. *Mar. Chem.* 86, 65–88.
- Belicka, L.L., Macdonald, R.W., Yunker, M.B., Harvey, H.R., 2004b. The role of depositional regime on carbon transport and preservation in Arctic Ocean sediments. *Mar. Chem.* 86, 65–88.
- Blattmann, T.M., Zhang, Y., Zhao, Y., Wen, K., Lin, S., Li, J., Wacker, L., Haghpor, N., Plötze, M., Liu, Z., 2018. Contrasting fates of petrogenic and biogenic carbon in the South China Sea. *Geophys. Res. Lett.* 45, 9077–9086.
- Boetius, A., Albrecht, S., Bakker, B., Bienhold, C., Felden, J., Fernández-Méndez, M., Hendricks, S., Katlein, C., Lalande, C., Krumpal, T., 2013. Export of algal biomass from the melting Arctic Sea ice. *Science* 339, 1430–1432.
- Bröder, L., Davydova, A., Davydov, S., Zimov, N., Haghpor, N., Eglinton, T.I., Vonk, J. E., 2020. Particulate organic matter dynamics in a permafrost headwater stream and the Kolyma River mainstem. *J. Geophys. Res. Biogeosci.* 125, e2019JG005511.
- Brown, K.A., McLaughlin, F., Tortell, P.D., Varela, D.E., Yamamoto-Kawai, M., Hunt, B., Francois, R., 2014. Determination of particulate organic carbon sources to the surface mixed layer of the Canada Basin, Arctic Ocean. *J. Geophys. Res. Oceans* 119, 1084–1102.
- Buesseler, K.O., 1998. The decoupling of production and particulate export in the surface ocean. *Glob. Biogeochem. Cycles* 12, 297–310.
- Burdige, D.J., 2007. Preservation of organic matter in marine sediments: controls, mechanisms, and an imbalance in sediment organic carbon budgets? *Chem. Rev.* 107, 467–485.
- Caesar, L., McCarthy, G., Thornalley, D., Cahill, N., Rahmstorf, S., 2021. Current Atlantic meridional overturning circulation weakest in last millennium. *Nat. Geosci.* 14, 118–120.
- Cai, W.-J., Chen, L., Chen, B., Gao, Z., Lee, S.H., Chen, J., Pierrot, D., Sullivan, K., Wang, Y., Hu, X., 2010. Decrease in the CO₂ uptake capacity in an ice-free Arctic Ocean basin. *Science* 329, 556–559.
- Cartapanis, O., Bianchi, D., Jaccard, S.L., Galbraith, E.D., 2016. Global pulses of organic carbon burial in deep-sea sediments during glacial maxima. *Nat. Commun.* 7, 1–7.
- Clement Kinney, J., Maslowski, W., Osinski, R., Jin, M., Frants, M., Jeffery, N., Lee, Y.J., 2020. Hidden production: on the importance of pelagic phytoplankton blooms beneath Arctic sea ice. *J. Geophys. Res. Oceans* 125, e2020JC016211.
- Close, H.G., 2019. Compound-specific isotope geochemistry in the ocean. *Annu. Rev. Mar. Sci.* 11, 27–56.
- Coachman, L.K., Aagaard, K., 1966. On the water exchange through Bering Strait 1. *Limnol. Oceanogr.* 11, 44–59.
- Coffin, R.B., Smith, J.P., Yoza, B., Boyd, T.J., Montgomery, M.T., 2017. Spatial variation in sediment organic carbon distribution across the Alaskan Beaufort Sea Shelf. *Energies* 10, 1265.
- Cooper, L.W., Savvichev, A.S., Grebmeier, J.M., 2015. Abundance and production rates of heterotrophic bacterioplankton in the context of sediment and water column processes in the Chukchi Sea. *Oceanography* 28, 84–99.
- Corlett, W.B., Pickart, R.S., 2017. The Chukchi slope current. *Prog. Oceanogr.* 153, 50–65.
- Darby, D.A., Ortiz, J.D., Polyak, L., Lund, S.P., Jakobsson, M., Woodgate, R.A., 2009. The role of currents and sea ice in both slowly deposited Central Arctic and rapidly deposited Chukchi–Alaskan margin sediments. *Glob. Planet. Chang.* 68, 58–72.
- Drenzek, N.J., Montluçon, D.B., Yunker, M.B., Macdonald, R.W., Eglinton, T.I., 2007. Constraints on the origin of sedimentary organic carbon in the Beaufort Sea from coupled molecular ¹³C and ¹⁴C measurements. *Mar. Chem.* 103, 146–162.
- Eicken, H., Gradinger, R., Gaylord, A., Mahoney, A., Rigor, I., Melling, H., 2005. Sediment transport by sea ice in the Chukchi and Beaufort Seas: increasing importance due to changing ice conditions? *Deep-Sea Res. II Top. Stud. Oceanogr.* 52, 3281–3302.
- Faust, J.C., Tessin, A., Fisher, B.J., Zindorf, M., Papadaki, S., Hendry, K.R., Doyle, K.A., März, C., 2021. Millennial scale persistence of organic carbon bound to iron in Arctic marine sediments. *Nat. Commun.* 12, 1–9.
- Goni, M.A., Yunker, M.B., Macdonald, R.W., Eglinton, T.I., 2005. The supply and preservation of ancient and modern components of organic carbon in the Canadian Beaufort Shelf of the Arctic Ocean. *Mar. Chem.* 93, 53–73.
- Goni, M.A., Juranek, L.W., Sipler, R.E., Welch, K.A., 2021. Particulate organic matter distributions in the water column of the Chukchi Sea during late summer. *J. Geophys. Res. Oceans* 126, e2021JC017664.
- Grebmeier, J., Cooper, L.W., 2019. Surface sediment samples collected from the CCGS *Sir Wilfrid Laurier* 2018, Northern Bering Sea to Chukchi Sea. Arctic Data Center. <https://doi.org/10.18739/A2C824F2J>.
- Guo, L., Macdonald, R.W., 2006. Source and transport of terrigenous organic matter in the upper Yukon River: evidence from isotope (^δ13C, ^Δ14C, and ^δ15N) composition of dissolved, colloidal, and particulate phases. *Glob. Biogeochem. Cycles* 20.
- Harada, N., 2016. Potential catastrophic reduction of sea ice in the western Arctic Ocean: its impact on biogeochemical cycles and marine ecosystems. *Glob. Planet. Chang.* 136, 1–17.
- Heip, C., Goosen, N., Herman, P., Kromkamp, J., Middelburg, J., Soetaert, K., 1995. Production and consumption of biological particles in temperate tidal estuaries. *Oceanogr. Mar. Biol.* 33, 1–149.
- Hill, V., Ardyna, M., Lee, S.H., Varela, D.E., 2018. Decadal trends in phytoplankton production in the Pacific Arctic Region from 1950 to 2012. *Deep-Sea Res. II Top. Stud. Oceanogr.* 152, 82–94.
- Hilton, R.G., Galy, A., Hovius, N., Hornig, M.-J., Chen, H., 2010. The isotopic composition of particulate organic carbon in mountain rivers of Taiwan. *Geochim. Cosmochim. Acta* 74, 3164–3181.
- Hu, A., Meehl, G.A., Ottobliessner, B.L., Waelbroeck, C., Han, W., Loutre, M., Lambeck, K., Mitrovica, J.X., Rosenbloom, N.A., 2010. Influence of Bering Strait flow and North Atlantic circulation on glacial sea-level changes. *Nat. Geosci.* 3, 118–121.
- Jahn, A., Holland, M.M., Kay, J.E., 2024. Projections of an ice-free Arctic Ocean. *Nat. Rev. Earth Environ.* 5, 164–176.
- Jakobsson, M., Pearce, C., Cronin, T., Backman, J., Anderson, L., Barrientos, N., Björk, G., Coxall, H., De Boer, A., Mayer, L., Mörth, C.-M., Nilsson, J., Rattray, J., Stranne, C., Semiletov, I., Regan, M., 2017. Post-glacial flooding of the Beringia Land Bridge dated to 11,000 cal yrs BP based on new geophysical and sediment records. *Clim. Past Discuss.* 1–22.
- Kolesnik, A., Astakhov, A., Kolesnik, O., 2017. Recent deposition environments in the Chukchi Sea and adjacent areas of the Arctic Ocean: evidence from Q-cluster analysis of sediment compositions and grain sizes. *Russ. Geol. Geophys.* 58, 1468–1477.
- Kurek, J., Cwynar, L.C., Vermaire, J.C., 2009. A late Quaternary paleotemperature record from Hanging Lake, northern Yukon Territory, eastern Beringia. *Quat. Res.* 72, 246–257.
- Lalonde, C., Grebmeier, J.M., Hopcroft, R.R., Danielson, S.L., 2020. Annual cycle of export fluxes of biogenic matter near Hanna Shoal in the northeast Chukchi Sea. *Deep-Sea Res. II Top. Stud. Oceanogr.* 104730.
- Laney, S.R., Krishfield, R.A., Toole, J.M., 2017. The euphotic zone under Arctic Ocean sea ice: vertical extents and seasonal trends. *Limnol. Oceanogr.* 62, 1910–1934.
- Lazar, K., Polyak, L., 2016. Pleistocene benthic foraminifers in the Arctic Ocean: implications for sea-ice and circulation history. *Mar. Micropaleontol.* 126, 19–30.
- Li, H., Lin, L., Song, P., Li, Y., Zhang, R., Lin, H., Lin, R., Hao, Q., Zhang, F., Zhang, G., 2017. Advances in Chinese Arctic and subarctic research in marine biology and ecology with emphasis on the Pacific Arctic sector. *Adv. Polar Sci.* 28, 111–119.
- Li, Z., Zhang, Y.G., Torres, M., Mills, B.J., 2023. Neogene burial of organic carbon in the global ocean. *Nature* 613, 90–95.
- Liu, Y., Ren, P., Song, T., Hillaire-Marcel, C., Zhang, X., Wang, X., 2023. Pacific Water impacts the burial of black and total organic carbon on the Chukchi Sea shelf, Arctic Ocean. *Palaeogeogr. Palaeoclimatol. Palaeoecol.* 621, 111575.
- Martens, J., Wild, B., Pearce, C., Tesi, T., Andersson, A., Bröder, L., O'Regan, M., Jakobsson, M., Sköld, M., Gemery, L., 2019. Remobilization of old permafrost carbon to Chukchi Sea sediments during the end of the last deglaciation. *Glob. Biogeochem. Cycles* 33, 2–14.
- Martens, J., Romankevich, E., Semiletov, I., Wild, B., van Dongen, B., Vonk, J., Tesi, T., Shakhova, N., Dudarev, O.V., Kosmach, D., 2021. CASCADE–The Circum-Arctic Sediment CArbon DatabasE. *Earth Syst. Sci. Data* 13, 2561–2572.
- McKay, J., de Vernal, A., Hillaire-Marcel, C., Not, C., Polyak, L., Darby, D., 2008. Holocene fluctuations in Arctic Sea-ice cover: dinocyst-based reconstructions for the eastern Chukchi Sea. *Can. J. Earth Sci.* 45, 1377–1397.
- Melsheimer, C., 2019. ASI Version 5 Sea Ice Concentration User Guide. University of Bremen, Institute of Environmental Physics, Bremen, Germany.
- Melsheimer, C., Spreen, G., 2019. AMSR2 ASI Sea Ice Concentration Data. Antarctic, Version 5.
- Moran, S., Ellis, K., Smith, J., 1997. ²³⁴Th/²³⁸U disequilibrium in the Central Arctic Ocean: implications for particulate organic carbon export. *Deep-Sea Res. II Top. Stud. Oceanogr.* 44, 1593–1606.
- Naidu, A., Cooper, L., Finney, B., Macdonald, R., Alexander, C., Semiletov, I.P., 2000. Organic carbon isotope ratios (^δ13C) of Arctic Amerasian continental shelf sediments. *Int. J. Earth Sci.* 89, 522–532.
- Nguyen, T.T., Zakem, E.J., Ebrahimi, A., Schwartzman, J., Caglar, T., Amarnath, K., Alcolombri, U., Peudecerf, F.J., Hwa, T., Stocker, R., 2022. Microbes contribute to setting the ocean carbon flux by altering the fate of sinking particulates. *Nat. Commun.* 13, 1–9.
- Nürnberg, D., Wollenburg, I., Dethleff, D., Eicken, H., Kassens, H., Letzig, T., Reimnitz, E., Thiede, J., 1994. Sediments in Arctic Sea ice: implications for entrainment, transport and release. *Mar. Geol.* 119, 185–214.
- Obrezkova, M., Pospelova, V.Y., 2019. Distribution of diatoms and dinocysts in surface sediments from the East Siberian and Chukchi Seas. *Paleontol. J.* 53, 790–794.
- O'Daly, S.H., Danielson, S.L., Hardy, S.M., Hopcroft, R.R., Lalonde, C., Stockwell, D.A., McDonnell, A.M., 2020. Extraordinary carbon fluxes on the shallow Pacific Arctic shelf during a remarkably warm and low sea ice period. *Front. Mar. Sci.* 7, 986.
- Ortiz, J.D., Polyak, L., Grebmeier, J.M., Darby, D., Eberl, D.D., Naidu, S., Nof, D., 2009. Provenance of Holocene sediment on the Chukchi-Alaskan margin based on combined diffuse spectral reflectance and quantitative X-Ray Diffraction analysis. *Glob. Planet. Chang.* 68, 73–84.

- Overeem, I., Nienhuis, J.H., Piliouras, A., 2022. Ice-dominated Arctic deltas. *Nat. Rev. Earth Environ.* 1–16.
- Pearson, A., McNichol, A.P., Benitez-Nelson, B.C., Hayes, J.M., Eglinton, T.I., 2001. Origins of lipid biomarkers in Santa Monica Basin surface sediment: a case study using compound-specific $\Delta 14C$ analysis. *Geochim. Cosmochim. Acta* 65, 3123–3137.
- Peng, G., Matthews, J.L., Wang, M., Vose, R., Sun, L., 2020. What do global climate models tell us about future Arctic Sea ice coverage changes? *Climate* 8, 15.
- Pickart, R.S., Pratt, L.J., Torres, D.J., Whitley, T.E., Proshutinsky, A.Y., Aagaard, K., Agnew, T.A., Moore, G., Dail, H.J., 2010. Evolution and dynamics of the flow through Herald Canyon in the western Chukchi Sea. *Deep-Sea Res. II Top. Stud. Oceanogr.* 57, 5–26.
- Pirtle-Levy, R., Grebmeier, J.M., Cooper, L.W., Larsen, I.L., 2009. Chlorophyll a in Arctic sediments implies long persistence of algal pigments. *Deep-Sea Res. II Top. Stud. Oceanogr.* 56, 1326–1338.
- Polyak, L., Belt, S.T., Cabedo-Sanz, P., Yamamoto, M., Park, Y.-H., 2016. Holocene Sea-ice conditions and circulation at the Chukchi-Alaskan margin, Arctic Ocean, inferred from biomarker proxies. *The Holocene* 26, 1810–1821.
- Ransom, B., Kim, D., Kastner, M., Wainwright, S., 1998. Organic matter preservation on continental slopes: importance of mineralogy and surface area. *Geochim. Cosmochim. Acta* 62, 1329–1345.
- Ren, J., Chen, J., Bai, Y., Sicre, M.-A., Yao, Z., Lin, L., Zhang, J., Li, H., Wu, B., Jin, H., 2020. Diatom composition and fluxes over the Northwind Ridge, western Arctic Ocean: impacts of marine surface circulation and sea ice distribution. *Prog. Oceanogr.* 186, 102377.
- Sarkar, S., Rahman, A., Khan, M.A., Rathi, A., Ragavan, P., Singh, A., Kumar, S., 2024. Isotopic evidence for degradation of particulate black carbon in the ocean. *Geophys. Res. Lett.* 51, e2023GL106050.
- Schubert, C.J., Calvert, S.E., 2001. Nitrogen and carbon isotopic composition of marine and terrestrial organic matter in Arctic Ocean sediments: implications for nutrient utilization and organic matter composition. *Deep-Sea Res. I Oceanogr. Res. Pap.* 48, 789–810.
- Semiletov, I., Pipko, I., Gustafsson, Ö., Anderson, L.G., Sergienko, V., Pugach, S., Dudarev, O., Charkin, A., Gukov, A., Bröder, L., 2016. Acidification of East Siberian Arctic Shelf waters through addition of freshwater and terrestrial carbon. *Nat. Geosci.* 9, 361–365.
- Sohail, T., Zika, J.D., Irving, D.B., Church, J.A., 2022. Observed poleward freshwater transport since 1970. *Nature* 602, 617–622.
- Soong, J.L., Castanha, C., Pries, C.E.H., Ofiti, N., Porras, R.C., Riley, W.J., Schmidt, M.W., Torn, M.S., 2021. Five years of whole-soil warming led to loss of subsoil carbon stocks and increased CO₂ efflux. *Sci. Adv.* 7, eabd1343.
- Søreide, J.E., Hop, H., Carroll, M.L., Falk-Petersen, S., Hegseth, E.N., 2006. Seasonal food web structures and sympagic–pelagic coupling in the European Arctic revealed by stable isotopes and a two-source food web model. *Prog. Oceanogr.* 71, 59–87.
- Stabeno, P.J., Mordy, C.W., Sigler, M.F., 2020. Seasonal patterns of near-bottom chlorophyll fluorescence in the eastern Chukchi Sea: 2010–2019. *Deep-Sea Res. II Top. Stud. Oceanogr.* 177, 104842.
- Stein, R., Macdonald, R.W., 2004. *The Organic Carbon Cycle in the Arctic Ocean*. Springer, Verlag Berlin Heidelberg.
- Stein, R., Fahl, K., Schade, I., Manerung, A., Wassmuth, S., Niessen, F., Nam, S.I., 2017. Holocene variability in sea ice cover, primary production, and Pacific-Water inflow and climate change in the Chukchi and East Siberian Seas (Arctic Ocean). *J. Quat. Sci.* 32, 362–379.
- Swärd, H., O'Regan, M., Pearce, C., Semiletov, I., Stranne, C., Tarras, H., Jakobsson, M., 2018. Sedimentary proxies for Pacific water inflow through the Herald Canyon, western Arctic Ocean. *arkots* 4, 19.
- Taylor, P.C., Boeke, R.C., Boisvert, L.N., Feldl, N., Henry, M., Huang, Y., Langen, P., Liu, W., Pithan, F., Sejas, S., 2021. Process Drivers, Inter-Model Spread, and the Path Forward: A Review of Amplified Arctic Warming.
- Viscosi-Shirley, C., Mammone, K., Piasias, N.G., Dymond, J., 2003. Clay mineralogy and multi-element chemistry of surface sediments on the Siberian-Arctic shelf: implications for sediment provenance and grain size sorting. *Cont. Shelf Res.* 23, 1175–1200.
- Vonk, J.E., Sánchez-García, L., Semiletov, I.P., Dudarev, O.V., Eglinton, T.I., Andersson, A., Gustafsson, Ö., 2010. Molecular and radiocarbon constraints on sources and degradation of terrestrial organic carbon along the Kolyma paleoriver transect, East Siberian Sea. *Biogeosciences* 7, 3153–3166.
- Walt, M., Ted, S., Mark, S., Julienne, S., 2020. Arctic Sea Ice News & Analysis. <http://nsidc.org/>.
- Watanabe, E., Onodera, J., Harada, N., Honda, M.C., Kimoto, K., Kikuchi, T., Nishino, S., Matsuno, K., Yamaguchi, A., Ishida, A., 2014. Enhanced role of eddies in the Arctic marine biological pump. *Nat. Commun.* 5, 1–12.
- Winsor, P., Chapman, D.C., 2004. Pathways of Pacific water across the Chukchi Sea: a numerical model study. *J. Geophys. Res. Oceans* 109.
- Woodgate, R.A., 2018. Increases in the Pacific inflow to the Arctic from 1990 to 2015, and insights into seasonal trends and driving mechanisms from year-round Bering Strait mooring data. *Prog. Oceanogr.* 160, 124–154.
- Xiang, Y., Lam, P.J., 2020. Size-fractionated compositions of marine suspended particles in the Western Arctic Ocean: lateral and vertical sources. *J. Geophys. Res. Oceans* 125, e2020JC016144.
- Yamamoto, M., Okino, T., Sugisaki, S., Sakamoto, T., 2008. Late Pleistocene changes in terrestrial biomarkers in sediments from the Central Arctic Ocean. *Org. Geochem.* 39, 754–763.
- Yamamoto, M., Nam, S.-I., Polyak, L., Kobayashi, D., Suzuki, K., Irino, T., Shimada, K., 2017. Holocene dynamics in the Bering Strait inflow to the Arctic and the Beaufort Gyre circulation based on sedimentary records from the Chukchi Sea. *Clim. Past* 13, 1111.
- Yan, Y., Koplík, J., 2009. Transport and sedimentation of suspended particles in inertial pressure-driven flow. *Phys. Fluids* 21, 013301.
- Yu, X., Ye, L., Bian, Y., Liu, Y., Zhang, W., Wang, W., Yao, X., Zhu, J., Jin, X., Wang, R., 2023. Composition and sources of suspended particles in the Pacific Arctic region. *Mar. Environ. Res.* 191, 106127.
- Yunker, M.B., Macdonald, R.W., Snowdon, L.R., Fowler, B.R., 2011. Alkane and PAH biomarkers as tracers of terrigenous organic carbon in Arctic Ocean sediments. *Org. Geochem.* 42, 1109–1146.
- Zeebe, R.E., Wolf-Gladrow, D., 2001. *CO₂ in Seawater: Equilibrium, Kinetics, Isotopes*. Gulf Professional Publishing.
- Zweng, M., Seidov, D., Boyer, T., Locarnini, M., Garcia, H., Mishonov, A., Baranova, O., Weathers, K., Paver, C., Smolyar, I., 2019. *World Ocean Atlas 2018, Volume 2: Salinity*.